TRIBHUVAN UNIVERSITY

INSTITUTE OF ENGINEERING

PULCHOWK CAMPUS

Thesis No:S004/075

SEISMIC VULNERABILITY ASSESSMENT OF A RESIDENTIAL STEEL BUILDING CONSIDERING SOIL STRUCTURE INTERACTION

By

Kailash Chaudhary

(075/MSStE/004)

A THESIS REPORT

SUBMITTED TO THE DEPARTMENT OF CIVIL ENGINEERING

IN PARTIAL FULFILLMENT OF THE REQUIREMENT FOR THE DEGREE OF

MASTER OF SCIENCE IN

STRUCTURAL ENGINEERING

DEPARTMENT OF CIVIL ENGINEERING

LALITPUR, NEPAL

SEPT, 2021

COPYRIGHT

The author has agreed that the library, Department of Civil Engineering, Pulchowk Campus, Institute of Engineering may make this thesis freely available for inspection. Moreover, the author has agreed that permission for extensive copying of this thesis for scholarly purpose may be granted by the professor(s) who supervised the work recorded herein or, in their absence, by the Head of the Department wherein the thesis was done. It is understood that the recognition will be given to the author of this thesis and to the Department of Civil Engineering, Pulchowk Campus, Institute of Engineering in any use of the material of this thesis. Copying or publication or the other use of this thesis for financial gain without approval of the Department of Civil Engineering, Pulchowk Campus, Institute of Engineering and author's written permission is prohibited. Request for permission to copy or to make any other use of the material in this thesis in whole or in part should be addressed to:

…….

Head of Department

Department of Civil Engineering

Pulchowk Campus, Institute of Engineering

Lalitpur, Nepal

TRIBHUVAN UNIVERSITY

INSTITUTE OF ENGINEERING

DEPARTMENT OF CIVIL ENGINEERING

PULCHOWK CAMPUS, PULCHOWK

The undersigned certify that they have read, and recommended to the Institute of Engineering for acceptance, a thesis entitled "**Seismic Vulnerability Assessment of a Residential Steel Building Considering Soil Structure Interaction**" submitted by Mr. Kailash Chaudhary (075/MSStE/004) in partial fulfillment of requirement for the degree of Master of Science in Structural Engineering.

Supervisor, Dr. Kshitij Charana Shrestha

Department of Civil Engineering

Institute of Engineering

Pulchowk Campus

Dr. Santosh Shrestha

External Examiner

Program Coordinator, Dr. Kamal Bahadur Thapa

Department of Civil Engineering

Institute of Engineering

Pulchowk Campus

ABSTRACT

The current practice for the design of the building structure is done by considering the footing as fixed footing. Designers approach fixed footing as the basis for design and hence neglect the effect of Soil Structure Interaction (SSI). This research focuses to understand the effect of SSI on the response of steel structure through the generation of validated models in SAP2000. Validation of SSI effect on steel structure is based on the experimentation done by Xiong et al. (2016). The validated model was utilized to study four real-scale residential steel buildings as case study. The bare frame is modelled and analyzed, using finite element method under two different boundary condition i.e., fixed base and SSI. From the results obtained, it shows that SSI clearly affects base shear and time period of the building. The vulnerability assessment of the case study prototype buildings is also done. The fragility curves generation approach is based on the concept of using pushover curve for capacity of the building and the demand is the obtained from response spectra of the building code. The fragility analysis highlights that SSI base models are relatively vulnerable in comparison to the fixed base models.

ACKNOWLEDGEMENT

Foremost, I would like to express my deepest and sincere appreciation to my supervisor Dr. Kshitij Charana Shrestha for the continuous guidance, motivation, encouragement, and suggestion throughout this research and thesis work.

I would also like to acknowledge all my respected teachers of Department of Civil Engineering for the guidance and concepts they gave me during my study at IOE, Pulchowk Campus.

I would like to express deep sense of gratitude to my friends Mr. Sagun Kandel, and Mr. Dhirendra Singh, Mr Naresh Subedi and 075 group for providing valuable study materials, cordial support, suggestions with kindness, enthusiasm, and dynamism which helped me in completing this task through various stages.

Last but not the least, I would like to thank my family and friends for their unending inspiration and invaluable support all throughout the study.

kailash chaudhary

(075/MSStE/004)

TABLE OF CONTENTS

LIST OF TABLES

LIST OF FIGURES

LIST OF SYMBOLS AND ABBREBIATIONS

K_z	Translation Stiffness along Z axis
K_y	Translation Stiffness along Yaxis
K_x	Translation Stiffness along X axis
K_{rx}	Rocking Stiffness about X axis
K_{rx}	Rocking Stiffness about Yaxis
K_t	Torsion about Zaxis
k_z	Dynamic translation Stiffness along Z axis
k_y	Dynamic translation Stiffness along Y axis
k_x	Dynamic translation Stiffness along X axis
k_{rx}	Dynamic rocking Stiffness about X axis
k_{rx}	Dynamic rocking Stiffness about Y axis
k_t	Dynamic torsion about Z axis
C_z	Damping along Z axis
C_y	Damping along Y axis
C_x	Damping along X axis
C_{rz}	Damping for rocking along Z axis
C_{ry}	Damping for rocking along Y axis
C_t	Damping for torsion about Z axis
$\bar{C_z}$	Dynamic damping along Z axis
$\bar{C_x}$	Dynamic damping along X axis
$\bar{C_y}$	Dynamic damping along Y axis
$\bar{C_{ry}}$	Dynamic damping for rocking along Y axis
$\bar{C_{rx}}$	Dynamic damping for rocking along X axis
$\bar{C_t}$	Dynamic damping for torsion along X axis
G	shear modulus
L	Half length of the footing
B	Half breadth of the footing
I_{bx}	area moment of inertia of soil-foundation contact along X axis
I_{by}	area moment of inertia of soil-foundation contact along Y axis
I_{bz}	polar moment of inertia of soil-foundation contact surface
A_b	area of the contact surface

a_0	dimensionless frequency factor
V_s	shear wave velocity
V_{la}	lysmer analog wave velocity
z	plastic section modulus
F_{ye}	expected yeild strength
L_C	length of member along which deformations are assumed
P	axial force in a member
P_{ye}	expected yield axial strength of a member
E	young's modulus of elasticity
I_b	moment of inertia of a beam
φ	normal cumulative distribution function
β_{eq}	equivalent viscous damping
β_o	hysteretic damping for equivalent viscous damping
E_D	energy dissipated by the structure in a single cycle of motion
E_{SO}	maximum strain energy associated with that cycle of motion
FEMA	Federal Emergency Management Agency
ATC	Applied Technology Council
SAP	Systems Applications and Products
SSI	Soil Structure Interaction
ASCE	American Society of Civil Engineers

CHAPTER-1 INTRODUCTION

1.1 Background

The seismic vulnerability of a structure is a quantity associated with its weakness in the case of earthquakes of given intensity, so that the value of this quantity and the knowledge of seismic hazard allows us to evaluate the expected damage from future earthquakes. The evolution of the vulnerability study in the world gave birth to several and historical center. The systemization of these vulnerability assessment approaches has been developed by many researchers and therefore differs due to varying levels of dependence of the following factors: nature and objective of the assessment, quality and availability of information, characteristics of the structure stock inspected, scale of assessment, methodology criteria, and degree of reliability of the expected results. Because of these differences, the coherence and consensus regarding the classification is always a contentious issue.

Vulnerability is assessed by a nonlinear static analysis. Displacement capacity curves (therefore deformability) are plotted for the buildings studied. These curves depend on the characteristics of these buildings and not a seismic load. The different degrees of damage corresponding to the displacements on the curve are located. By correlating the capacity curve of the displacement building with a maximum displacement caused by seismic motion of the soil given, determined by a proposed method in the document, a point called "performance point" is obtained. Its position, relative to the desired level of performance, indicates that this level is reached or not.

Performance level or limit state for the structural system is the point after which the structure is no longer capable of performing the desired functions. Performance levels can be identified by using qualitative or quantitative approach. Building codes generally follows qualitative approach. Three limit states (IO, LS and CP) are defined according to structure stiffness, strength and durability.

Most of civil engineering structures involve some type of structural element with direct contact with the ground. During the external forces, such as earthquake, acts on these systems, neither the structural displacements nor the ground displacements, are independent of each other. The response of the structure to earthquake shaking is affected

by interaction between three connected systems; the structure, the foundation and the soil underlying and surrounding the foundation and building. The process in which the response of the soil influences the motion of the structure and the motion of the structure influences the response of the soil is termed as Soil-Structure Interaction.

Implementing soil-structure interaction effects enable the designer to assess the real displacement of the soil-foundation system. Present design practice for seismic loading assumes the building to be fixed at their bases. Whereas, in truth supporting soil allows movement to some extent due to their natural ability to deform. This property of soil decreases the overall lateral stiffness of the structural system resulting in the lengthening of lateral natural periods. Today's structural design methods neglect the SSI effect but considering SSI increase the fundamental time period of the structure. So, change in the support condition of base of structure widely changes its design, and by modelling SSI behavior can be converses towards actual behavior.

On the other hand, distribution of element forces may be change due to SSI. For example, P-Δ effects could affect failure mechanism, and therefore the performance, of steel structures designed with normal criteria. Magnitude of these second order effects is highly dependent on the columns support condition. Consideration of flexible base may increase the magnitude and influence of P-Δ effects and affect failure mechanism these increments are neglected in the fixed base analysis.

Impedance functions ($\tilde{K}(\omega)$) are understood as the dynamic stiffness of soil foundation system. They can be defined as the dynamic force (or moment) needed to produce unitary displacement (or rotation) in a massless foundation. Because of their dynamic nature, impedance functions are frequency dependent complex quantities. Impedance functions can be expressed in its general form as:

$$\tilde{K}(\omega) = K(\omega) + i\omega C(\omega) \tag{1.1}$$

Where the real part ($K(\omega)$) represents the inertia and stiffness of soil-foundation system and the imaginary part ($C(\omega)$) represents the amount of energy dissipated by either wave radiation or hysteretic behavior of soil.

Since the impedance functions definition considers the whole soil-foundation system performing together, the representation of soil-foundation stiffness and damping is done by a set of equivalent springs and dashpots on the base of the building. Ground motions that are not influenced by the presence of ground structures are referred as free field motions. When a structure founded on solid rock is subjected to an earthquake, the extremely high stiffness of the rock constrains the rock motion to be very close to the free field. Structure founded on rock are considered to be fixed base structure.

On the other hand, the same structure would respond differently if supported on a soft soil deposit. First, the in ability of the foundation to conform to the deformation of the free field motion would cause the motion of the base of the structure to deviate from the free field motion. Second the dynamic response of the structure itself would induce deformation of the supporting soil. This process, in which the response of the soil influences the motion of the structure and the response of the structure influences the motion of the soil, is referred to as soil-structure interaction.

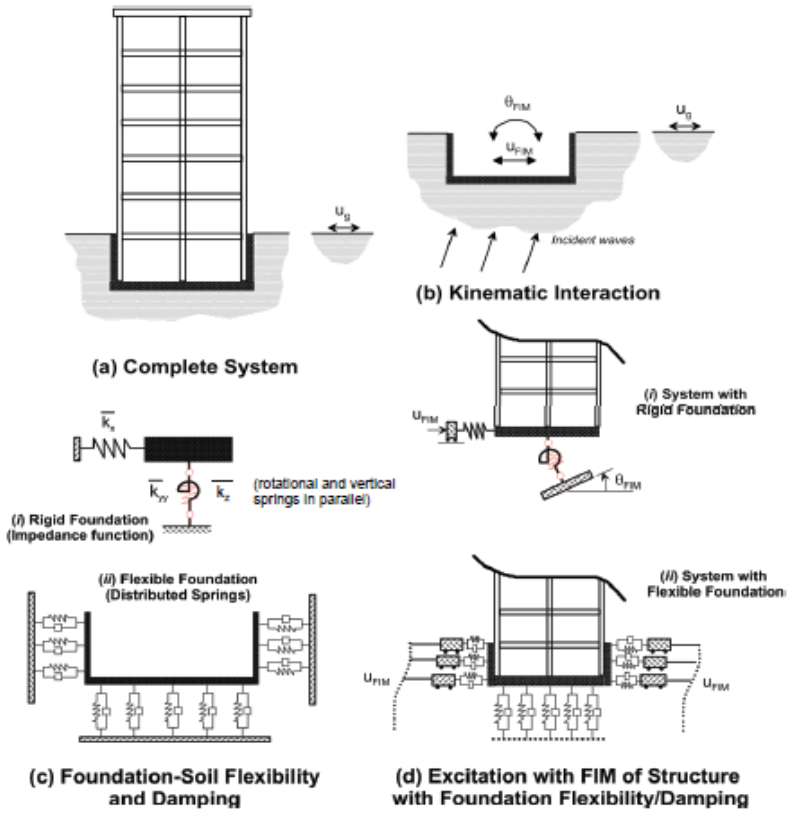

Figure 1-1: Schematic Illustration of a Substructure Approach to Analysis of Soil-Structure Interaction using (i)Rigid Foundation; or(ii) Flexible Foundation Assumptions(NIST,2012)

The soil can be represented by the stiffness and the damping coefficient by different relations and formula and among those Gazetas (1991) is also widely used. The formulae are illustrated in following chapter in Section 3.2.4.

Consider a single degree-of-freedom structure with stiffness k, and mass m, resting on a fixed base, as depicted in Figure1. T be the natural period of structure for this case. Then consider the same structure with vertical, horizontal, and rotational springs at its base, representing the effects of soil flexibility against a rigid foundation, as depicted in Figure 2. The vertical spring stiffness in the z direction is denoted k_z, the horizontal spring stiffness in the x direction is denoted k_x, and the rotational spring is denoted k_{yy}, representing rotation in the x-z plane (about the y-y axis). T̃ be the natural period of structure for flexible base. Schematic illustration of deflections caused by force applied to fixed base and structure with vertical, horizontal and rotational flexibility at is base in and Figure 1--3

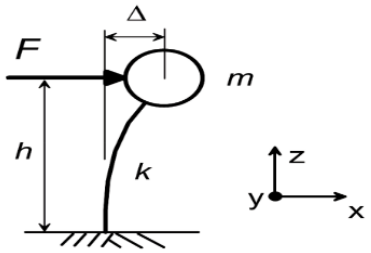

Figure 1-2: Fixed-Base Structure NIST(2012)

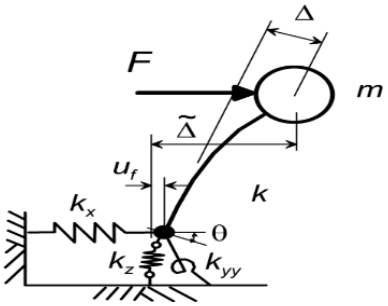

Figure 1-3: Structure with Vertical, Horizontal and Rotational Flexibility at its Base NIST(2012)

After simplification, we get classical period lengthening expression as:

$$\frac{\tilde{T}}{T} = \sqrt{1 + \frac{k}{k_x} + \frac{kh^2}{k_{yy}}} \qquad 1.2$$

The above expression for the period lengthening can be applied to multi degree of freedom structure by taking the height h as the center of mass for the first-mode shape. This height is approximately two-thirds of the overall structure height, and taken as 0.7 times the

height in ASCE/SEI 7-10. In such cases, period lengthening applies to only the first-mode only.

1.2 Need of Research

Steel building are being built on rapid pace both in commercial and residential. The designs rarely utilize SSI effect to check the response of structure. The prediction that the SSI will decrease the seismic response may not always be true. Thus, the actual seismic response should be used and also research on seismic vulnerability assessment of real-scale steel buildings considering SSI is not carried out till date in Nepal.

1.3 Objective of Research

The objectives of this research are as follows:

i. To compare the seismic response of the steel building founded on fixed based and on SSI case.
ii. To assess the vulnerability of the selected prototype residential steel buildings thorough fragility curves.

1.4 Scope

The scope of this research are as follows:

i. The proposed study contributes to understand the present scenario of rapidly built residential steel buildings.
ii. The study highlights the importance of considering SSI effect for steel structure.

1.5 Limitation of the Study

The limitation of the study are listed below:

i. The soil considered is non liquefiable soil.
ii. Geometric nonlinearity (P- delta effect) is not considered.

1.6 Thesis Organization

This thesis work has been mainly organized in six chapters.

Chapter 1 gives an introduction to the thesis. It also highlights the need of the study, objective of research and scope of this thesis work.

Chapter 2 presents the comprehensive literature reviewed during the research. This includes literature review for soil structure interaction and vulnerability assessment of steel building.

Chapter 3 describes the validation, techniques and methodology used for push over analysis and seismic vulnerability assessment.

Chapter 4 describes the building prototype, soil idealization, structural modelling, material properties, structural elements and loading. The results of research work are included in this chapter.

Chapter 5 gives the results and discussion of this research.

Chapter 6 gives the conclusion and recommendation of this research.

CHAPTER-2 REVIEW OF LITERATURE

2.1 Literature Review

Literature review is carried out as a part of this study to gain insight on the works to be carried out and to act as a guide for successful completion of this thesis work. The problems related with this work was identified and necessary reference were taken from the literatures shown below:

2.1.1 Soil Structure Interaction and its Effect

Wolf (1985) described about the dynamic soil structure interaction behavior. Taking soil-structure interaction into account will reduce the peak structural distortion for harmonic excitation, while for a specific frequency of the excitation the result can be either smaller or larger than that of the fixed-base structure. The design code considers the decrease in shear force due to flexibly supported soil considering the change from the fixed-base frequency to the fundamental frequency of the structure-soil system and the corresponding increase in the damping. He further added, the response spectra curves presented in seismic codes have been prepared considering fixed based SDOF model.

Gazetas (1991) presented simple algebraic formulas and dimensionless charts for estimating the dynamic impedances (springs and dashpots) of foundations, for all the significant translational and rotational modes of vibration. This paper presents a complete set of simple formulas and graphs covering nearly all foundation base shapes(excluding annular),surface and partially and fully embedded foundations, all significant modes of vibration and a fairly adequate frequency range, reasonably deep and uniform soil deposits that can be modelled as a homogenous half space. This paper presents the geometry of rigid but massless foundation. Two numerical examples illustrating the use of the formulas and graphs for surface and deep foundation are solved and explains the role of the foundation shape and the degree of the embedment on radiation damping for the various modes of the vibrations.

Xiong et.al (2015) performed a systematic experimental survey on a 1/4-scale, steel-frame model building with and without considering SSI and compared the results with its numerical counterpart obtained by using SAP2000. Adding or removing inter story diagonal and additional weights respectively, could change the stiffness and the mass of

the structure. A total of 34 scenarios were studied with the variation in overall stiffness and mass of the structure. In each experimental scenario, the fundamental time period of the structure was determined under fixed base and flexible base condition. The analytical basic periods of the structure with SSI was found in excellent agreement with that obtained both experimentally and numerically.

Tom P (2014) studied the effect of resonance on structures due to Soil Structure Interaction during earthquakes. Opposing to popular belief and codal provisions, SSI actually amplifies the seismic demand on structures by amplifying peak acceleration during an earthquake. During resonance all peak values of motion are amplified therefore, the values considered for design are inadequate. Such structures, although perhaps well designed, have a high probability of failure when the system resonates.

Chhetri and Thapa (2015) investigated about soil structure interaction and performed seismic design according codal provisions. It was concluded that it is very necessary to consider the effect of SSI for seismic design of building founded on soil with shear wave velocity less than or equal to 300 m/sec.

U.S. Department of Commerce (2012) investigated on soil structure interaction, and provides specific recommendations for modeling seismic soil structure interaction effects on building structures in engineering practice. U.S. Department of Commerce, (2012) represent progress in the state of SSI knowledge of practicing engineers. It provides a path to systematize the design with a consistent set of variable and units. Techniques are described by which SSI phenomena can be simulated in engineering practice, and specific recommendations for modeling seismic soil structure interaction effect on building structures are provided.

Thapa (2017) investigated about the soil structure interaction for Balaju and Sankhu site. The research was performed by converting soil to the equivalent spring for stiffness and dashpot for damping. Structure located at stronger soil has higher capacity compared to the corresponding structure located at weaker soil observed that top story displacement was more in case of SSI than in fixed base condition.

Pradhan (2002) performed SSI for 2,4,6,8 story with fixed spring base and FEM model of soil structure. He concluded that design is greatly affected by the method of analysis chosen, fixed base is more conservative.

Poudel (2020) performed the direct analysis method of SSI of soft story building in the Kathmandu valley. He found that capacity of the structure gets reduced considering the flexibility of soil. So, according to the present design approach considering buildings fixed at their base are being overestimated for resisting shear.

Chowdhury (2011) performed nonlinear soil structure analysis and studied seismic response of low rise steel moment resisting frame. Concluded that soil–structure interaction effect may play an important role in altering the force and displacement demand, indicating the necessity for consideration of inelastic foundation behavior in the modern design codes to accomplish a more economic yet safe structural design.

Shouping (2012) conducted test in the shock absorption laboratory with comprehensive artificial soil in Hunan University. The soil are 30.7m*6m*4m, no tank bottom soil and connected with the earth. He used SAP2000 steel frame model doing excitation on the rigid foundation and comparison with the tests of steel frame on soil tank. He concluded that soil-structure interaction is the influence of the natural period of structure, and on the soil tank the upper structure of stiffness increases, the structure additional period was increasing.

Awlla (2020) studied effect of fixed base and soil structure interaction on the dynamic response of steel structure. He concluded that SSI has significant impact on the dynamic response of the steel structure.

Sola (2014) studied dynamic soil structure interaction on the inelastic response of steel frames. Analysis of buildings under seismic actions with flexible base must take in to account the contribution to total displacement of two principal components: displacement introduced by structural deformation and displacement due to a rigid body behavior. Failure mechanism, over strength and ductility modifications due to dynamic soil structure interaction were analyzed by the comparison of the capacity curves of the frames with rigid (fixed) and flexible base.

2.1.2 Vulnerability Assessment of Steel Structures

FEMA (2003) HAZUS is a risk-estimation software developed by FEMA to calculate potential losses due to natural disasters. Federal, state, regional, and local government use the HAZUS-MH Earthquake Model for earthquake risk mitigation, preparedness, response, and recovery planning (FEMA, 2003). The earthquake component of HAZUS-MH applies a series of empirical ground motion attenuation relationships developed from source parameters of both regional and global historical earthquakes to estimate strong ground motion. Ground motion and resulting ground failure due to earthquakes are then used to calculate, direct physical damage for general building stock, essential facilities, and lifelines, including transportation systems and utility systems. Earthquake losses are expressed in structural, economic and social terms. Where available, comparisons between recorded earthquake losses and HAZUS-MH earthquake losses are used to determine how region coordinators can most effectively utilize their resources for earthquake risk mitigation

Annan et al. (2009) concluded that the severity of damage a building suffers depends on its vulnerability and the seismic hazard to which it is exposed. Vulnerability is controlled by the overall capacity of the building, which could be a function of the inter-story drift, plastic rotations, or member forces. Earthquake ground accelerations cause building response resulting in drifts and member forces, all of which can represent demands. If both the ground motion demand and the structure's capacity to resist this demand could be predicted with some certainty, then buildings could be designed with some level of confidence of performing as desired.

Porter (2021) provided a primer for earthquake-related fragility, vulnerability, and risk. He provided the guidelines for catastrophe risk modeling, such as users and consumers of catastrophe models by RMS, Applied Insurance Research, EQECAT, Global Earthquake Model, or the US Federal Emergency Management Agency (FEMA). He discussed damageability in terms of the occurrence of some undesirable event such as a building collapse that either occurs or does not occur. He discussed the three leading methods to derive vulnerability functions.

Wen et al. (2004) described the methods for the determination of the vulnerability functions framework for buildings (masonry, RCC and steel). The methodology included

systematic treatment of uncertainties in seismic excitation, dynamic response demand on lateral force resisting structure and the capacity of building structure in resisting limit states for immediate occupancy to incipient collapse. The study considered both the aleatory (randomness) and epistemic (modelling error) uncertainty in the demand and the capacity.

Genctruck et al. (2007) Improved fragility relationships for populations of buildings based on inelastic response analysis is performed in the absence of comprehensive and statically viable observational damage data. Here a new framework is proposed for deriving fragility relationships for populations of buildings. Thirty Six building type are considered while particular focus is placed on wood, steel, concrete and masonry frame structures is done by Capacity spectrum method. Capacity curve are generated from finite element based pushover analysis while demand is synthetically generated from ground motion of probable earthquake in USA. Structural assessment (CSM). Fragility curves are developed and its component like capacity, demand and structural response are based on rigorous analysis. Comparison of fragility curve with FEMA (2003) HAZUS fragility as well as from other studies were undertaken. They found that fragility curves based on analytical simulations and their consistent limit states are more reliable than relying on the expert opinions. They observed that the common trend in comparing the FEMA (2003) HAZUS and new fragility is that FEMA (2003) Hazus underestimates as the strength of the structure increases. Thus, mainly attributed to the high limit state threshold values in FEMA (2003) Hazus.

Summary of literature

Soil Structure Interaction and its importance

Gazetas(1991) illustrated different aspects of SSI and formulated the Spring Stiffness and the damping value for soil. The formulas and the chart as described by Gazetas(1991) were used in this thesis.

Xiong et al.(2015) performed experiment and modelled the samples in SAP2000 for verification.The thesis used Four samples and verified the results to validate the spring constant.

Poudel(2020) used direct method for SSI and for soil properties were obtained by sample conducting SPT test.

Chhetri and Thapa (2015) performed seismic design of mid-rise moment resistant building frame using SSI and used different parameters for soil and the values of the soil parameters are in the thesis.

Capacity Spectrum method:

Tripathi and Rai(2018)performed seismic vulnerability assessment and fragility analysis of stone masonry monastic temples using Capacity Spectrum Method and using response spectrum of IS1893(2016) and the thesis focus in the performance point using capacity spectrum using response spectrum of NBC 105(2020).

Chopra and Goel(1999) described different method of capacity spectrum methods.The thesis focus on using varying ductility in nonlinear range to find the performance point of the structure.

Gencturk et al.(2007) described different aspects of fragility generation using Hazus relation,Porter formulation, Wen et al(2004) and also deals with the evaluation of performance point using Capacity Spectrum Method.

ATC 40 deals with seismic evaluation and retrofit of concrete building and provides the different method of performance point. Here the thesis uses concept of Capacity Spectrum Method.

Fragility Curve generation

Wen et al(2004) defined a fragility function along with determination of vulnerability functions and use for masonry, reinforced cement concrete and steel building. The thesis uses the fragility function of Wen et al.(2004) for determination of fragility curve.

FEMA(2003) HAZUS illustrates the methodology which deals with nearly all aspects of built environment and a wide range of different types of losses includes buildings and bridges. The thesis grabs the limit state of damage for steel building for fragility curve generation.

CHAPTER-3 METHODOLOGY AND VALIDATION

3.1 Methodology

Figure 3-1 shows the general methodology adopted for the current research work. The steps followed are listed below: A comprehensive literature survey of modeling soil structure interaction and its application to steel structure is done. This was followed by development of validated FE model with consideration of SSI effect on steel structure. To accomplish the objectives of the thesis work, the following procedures are adopted:

i. Comprehensive review of various literature for modeling soil structure interaction and its application to steel structure.
ii. Development of validated FE model with consideration of SSI effect on steel structure.
iii. Selection and structural idealization for a prototype residential steel building
iv. Soil idealization: Two different FE models of the prototype steel structure is developed to be supported by non-liquefiable soil as follows:
    a. Conventional FE model with fixed support at the base
    b. SSI model with flexible support of soil at the base
v. Comparisons between the above two models are done in terms of natural period, seismic base shear, story displacement and story drift.
vi. The FE models are further subjected to nonlinear static pushover analysis.
vii. Determination of performance points for the FE models using Capacity Spectrum Method.
viii. Generation of fragility curve and comparison between the conventional and SSI model.

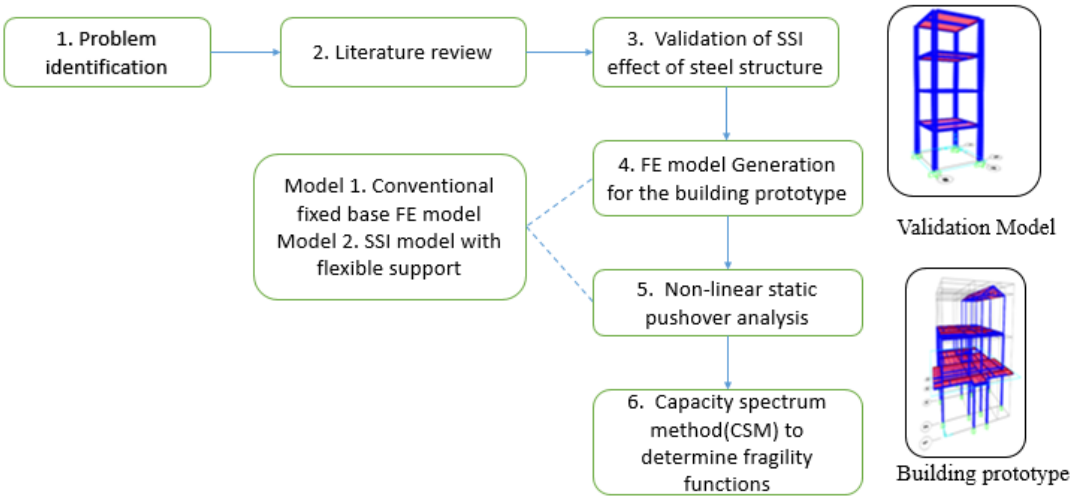

Figure 3-1: Methodology Flowchart and Work flow

3.2 Validation

Xiong et.al (2015) performed a comprehensive experimental program on several different 1/4-scaled steel-frame model building with and without considering SSI. The test prototype adopted by Xiong et al. (2015) was used to validate the developed finite element model in this study. The main purpose for validation focused on input values of spring stiffness and damping based on the particular site characteristics. The finite element model was developed in SAP2000V22.

3.2.1 Prototype Structure Idealization based on Xiong et.al (2015)

Building prototypes consisted of steel framed structures of 6 story and 4 story with 1 and 1.5m story height respectively and bay length of 1m. The thickness of slab plate was 10mm, with beams of dimension H100x50x5x7 and columns of H125x125x6.9x9. C20 grade of concrete was used with Q235 grade of steel sections.

3.2.2 Loadings

The prototype model has an area load of 1.51kN/m^2 on each floor. No other loads were considered except the dead load of the sections used on the model.

3.2.3 Soil Idealization

To obtain the values of the stiffness of the springs for the soil, density of the soil (ρ)1.64gm/m^3, poison's ratio (μ) 0.3 and shear wave velocity (v_s) 211 m/s were used. The values are based on data reported in Xiong et al. (2015).

3.2.4 Spring constants

The procedure to obtained dynamic springs constant from static spring constant used in this thesis is based on the Gazetas (1991) is presented in Figure 3-2.

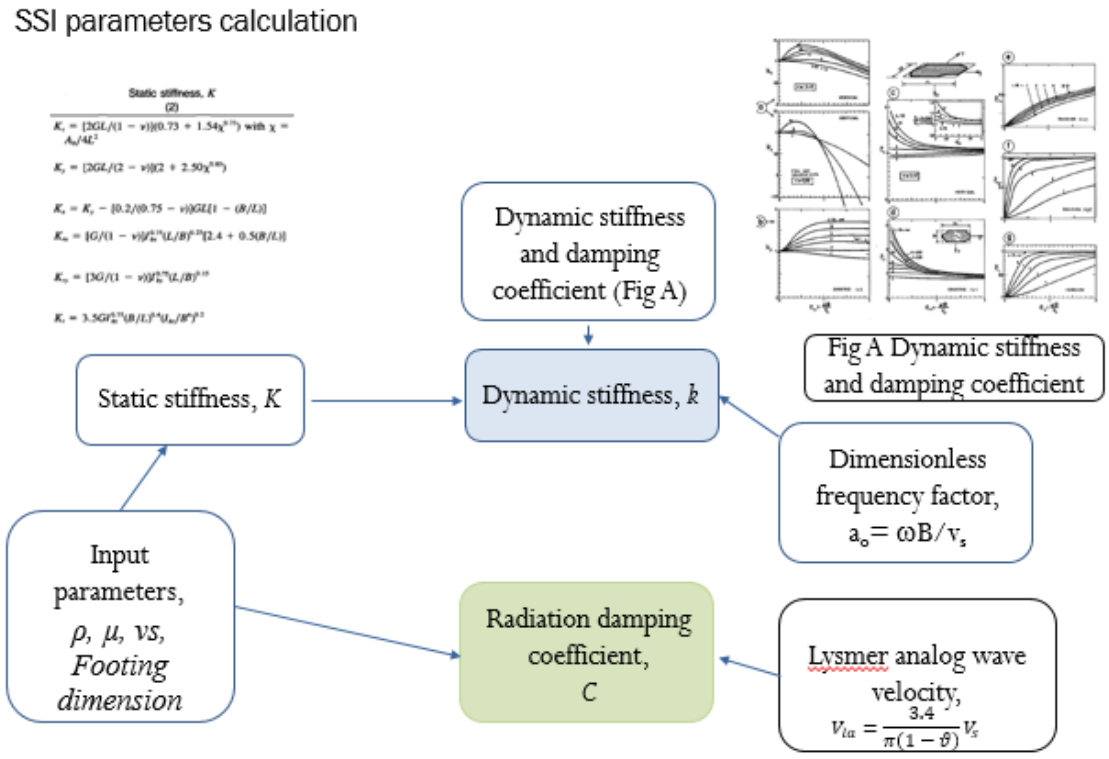

Figure 3-2: SSI parameters calculation for static stiffness, dynamic stiffness, static damping, and dynamic damping

The relation to obtain the spring constant values are given below:

Static stiffness

Translation along z axis

$$K_z = \left[\frac{2GL}{(1-\vartheta)}\right](0.73 + 1.54\chi^{0.75}) \; with \; = {}^{A_b}/_{4L} \qquad 3.1$$

Translation along

$$K_y = \left[\frac{2GL}{(1-\vartheta)}\right](2 + 2.5\chi^{0.85}) \qquad 3.2$$

y axis		
Translation along x axis	$K_x = K_y - \left[{}^{0.2}/_{(0.75-\vartheta)}\right] GL\left[1 - {}^{B}/_{L}\right]$	3.3
Rocking about x axis	$K_{rx} = \left[{}^{G}/_{(1-\vartheta)}\right] I_{bx}^{0.75}\left({}^{L}/_{B}\right)^{0.25}\left[2.4 + 0.5\left({}^{B}/_{L}\right)\right]$	3.4
Rocking about y axis	$K_{ry} = \left[{}^{3G}/_{(1-\vartheta)}\right] I_{by}^{0.75}\left({}^{L}/_{B}\right)^{0.15}$	3.5
Torsion about z axis	$K_t = 3.5GI_{bz}^{0.75}\left({}^{B}/_{L}\right)^{0.4}\left({}^{I_{bz}}/_{B^4}\right)$	3.6

Dynamic stiffness

Translation along z axis	$k_z = K_z\left({}^{L}/_{B}, \vartheta; a_0\right) is\ plotted\ in\ the\ fig 3-3(a)$	3.7
Translation along y axis	$k_y = K_y\left({}^{L}/_{B}; a_0\right) is\ plotted\ in\ the\ fig 3-3(b)$	3.8
Translation along x axis	$k_x = 1$	3..9
Rocking about x axis	$k_{rx} = 1 - 0.20a_0$	3.10
Rocking about y axis	$\vartheta < 0.4; k_{ry} = 1 - 0.26a_0$	3.11
Torsion about z axis	$k_t = 1 - 0.14a_0$	3.12

Damping

Translation along z axis

$$C_z = (\rho v_{la} A_b).\bar{c_z} \; where \; \bar{c_z} = \bar{c_z}\left({}^{L}/_{B}; a_0\right) \; as \; plotted \; in \; fig3-3(c) \quad 3.13$$

Translation along y axis

$$C_y = (\rho v_s A_b).\bar{c_y} \; where \; \bar{c_y} = \bar{c_y}\left({}^{L}/_{B}; a_0\right) \; as \; plotted \; in \; fig3-3(d) \quad 3.14$$

Translation along x axis

$$C_x = \rho v_s A_b \quad 3.15$$

Rocking about x axis

$$C_{rx} = (\rho v_{la} I_{bx}).\bar{c_{rx}} \; where \; \bar{c_{rx}} = \bar{c_{rx}}\left({}^{L}/_{B}; a_0\right) \; as \; plotted \; in \; fig3-3(e) \quad 3.16$$

Rocking about y axis

$$C_{ry} = \left(\rho v_{la} I_{by}\right).\bar{c_{ry}} \; where \; \bar{c_{ry}} = \bar{c_{ry}}\left({}^{L}/_{B}; a_0\right) \; as \; plotted \; in \; fig3-3(f) \quad 3.17$$

Torsion about z axis

$$C_t = (\rho v_{la} I_{bt}).\bar{c_t} \; where \; \bar{c_t} = \bar{c_t}\left({}^{L}/_{B}; a_0\right) \; as \; plotted \; in \; fig3-3(g) \quad 3.18$$

where,

G= shear modulus

L= Half length of the footing

B= Half breadth of the footing

I_{bx}= area moment of inertia of soil-foundation contact along X axis

I_{by}= area moment of inertia of soil-foundation contact along Y axis

I_{bz}= polar moment of inertia of soil-foundation contact surface

A_b= area of the contact surface

a_0=dimensionless frequency factor

V_s= shear wave velocity

V_{la}= lysmer analog wave velocity

The dimensionless graph for determining the dynamic stiffness and damping coefficients is given in Figure 3-3.

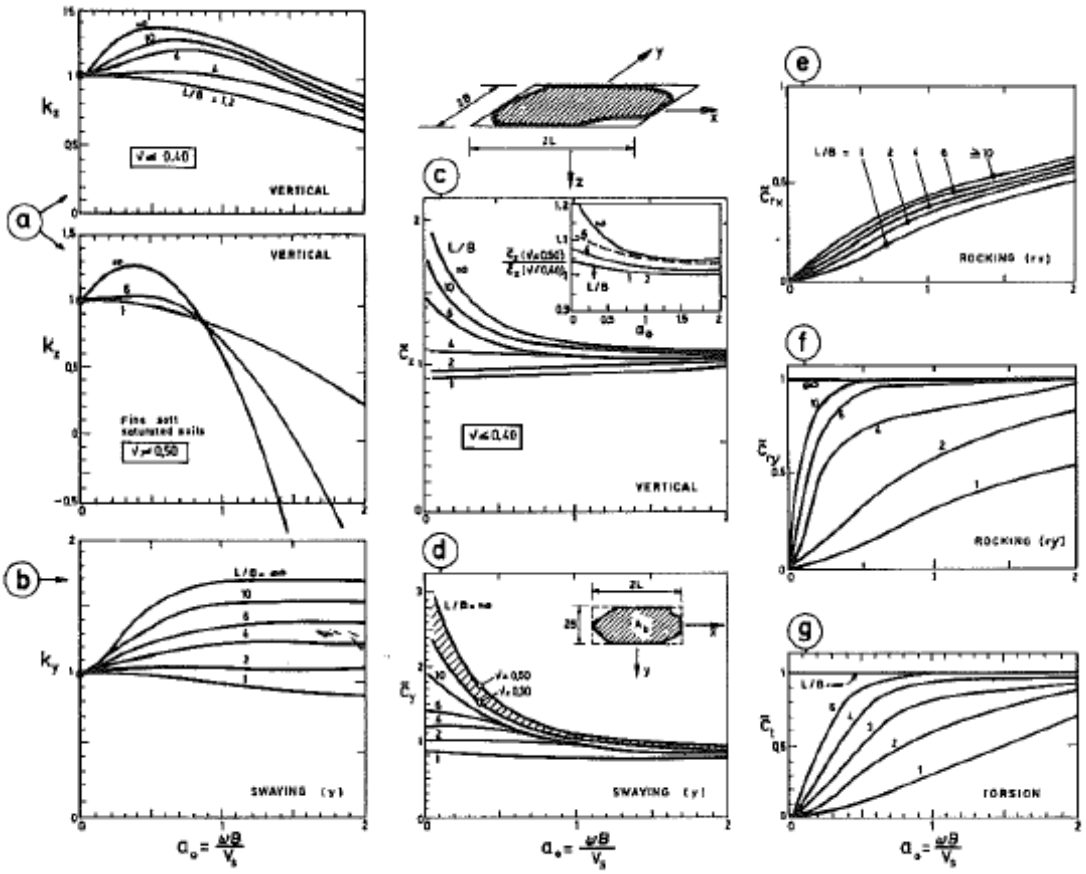

Figure 3-3: Dimensionless Graphs for Determining Dynamic Stiffness and Damping Coefficients of Surface Foundations (Gazetas, 1991)

Through the use of Equations 3.1 to 3.18 and Figure 3-3, the values for spring stiffnesses are given in Table 3-1 and damping constants are in Tale 3-2. These calculated spring constants were used as input parameter as links instead of fixed support in SAP2000V22 in corresponding SSI models.

Table 3-1: Dynamic Stiffness (kN/m^2)

k_z	k_x	k_y	k_{rx}	k_{ry}	k_{rz}
114836.1	92771.3	92771.3	92059.2	946833.4	160067.8

Table 3-2: Damping Constant (N/m/s)

c_z	c_x	c_y	c_{rx}	c_{ry}	c_{rz}
535275.7	311436	346040	17842.52	21411.02	23069.3

3.2.5 Prototype models for validation using SAP2000

The following cases were modelled in SAP2000V22 for fixed support and flexible support cases as shown in Figure 3-4 and Figure 3-5 respectively:

Case 1. without load and floor height 1 m

Case 2. with load and floor height 1 m

Case 3. without load and floor height 1.5 m

Case 4. with load and floor height 1.5 m

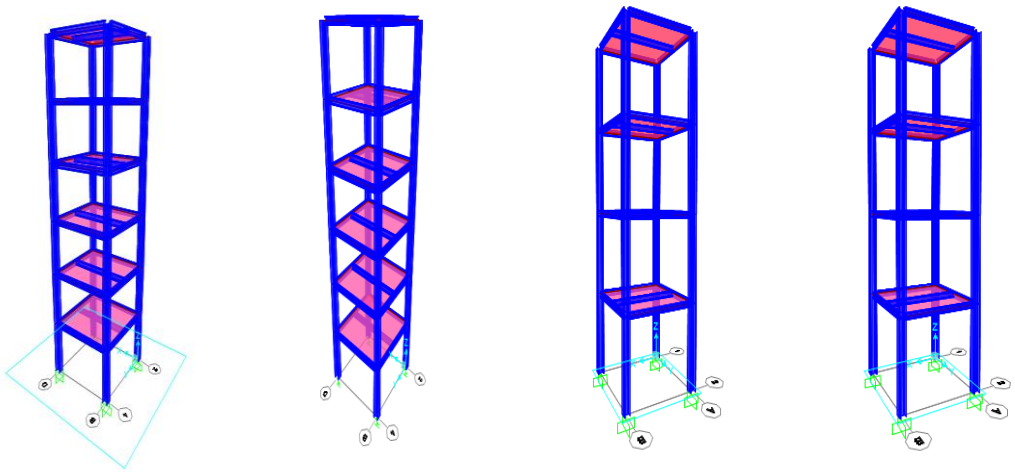

Case 1 Case 2 Case 3 Case 4

Figure 3-4: Prototype models in SAP2000 with fixed support

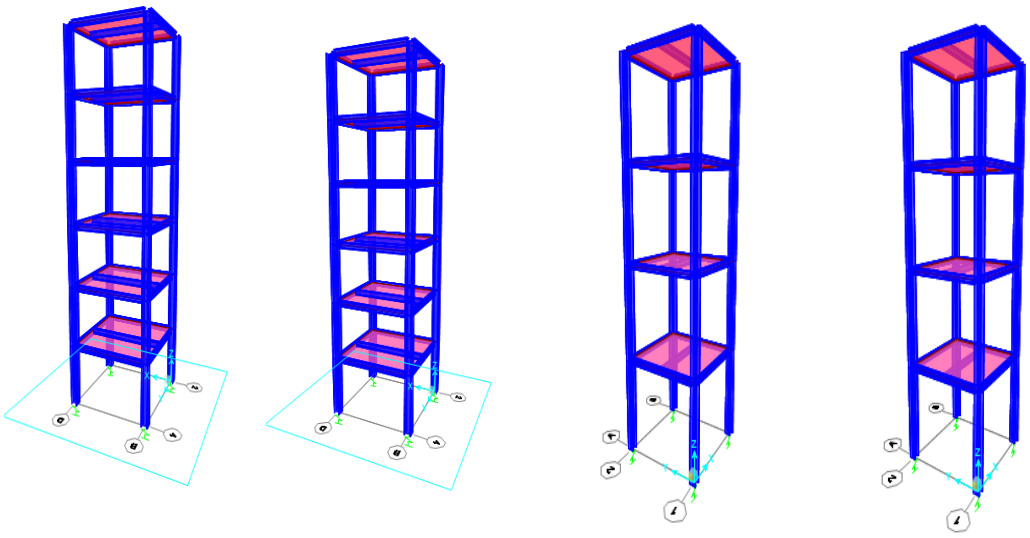

Case 1 Case 2 Case 3 Case 4

Figure 3-5: Prototype models in SAP2000 with flexible support

3.2.6 Comparison of Fundamental Time Period from Experiment with SAP 2000

Table 3-3 shows the comparison of results for the fundamental time periods. The time periods obtained from SAP were comparable with the experimental results with average percentage of variation of 5.3% for fixed based models and 9.3% for SSI models. Similar

procedures were followed with the spring coefficients relations given by Gazetas, 1991 to generate the SSI based models for the real-scale building in the following chapters**.**

Table 3-3: Comparison of Fundamental Time Period from Experiment with SAP2000

		SAP results		Experimental		Variation (%)	
S.N.	Direction	Fixed(s)	SSI(s)	Fixed(s)	SSI(s)	Fixed	SSI
1	x	0.204	0.217	0.210	0.221	2.92	1.66
	y	0.300	0.305	0.310	0.342	3.51	10.75
2	x	0.260	0.275	0.288	0.304	9.93	9.62
	y	0.423	0.432	0.426	0.470	0.84	8.13
3	x	0.226	0.235	0.213	0.260	6.00	9.47
	y	0.423	0.428	0.377	0.393	12.11	8.89
4	x	0.276	0.287	0.297	0.352	6.88	18.47
	y	0.518	0.524	0.515	0.568	0.45	7.85

3.3 Pushover Analysis

Static pushover analysis is becoming a widespread tool to perform the seismic assessment of both existing and new structures. The static pushover analysis method has no strict theoretical base. It is mainly based on the assumption that the response of the structure is controlled by the first mode of vibration and mode shape, or by the first few modes of vibration, and that this shape remains constant throughout the elastic and inelastic response of the structure. Furthermore, the response of a MDOF structure is related to the response of an equivalent SDOF system. The earthquake induced motion of an elastic or inelastic MDOF system can be derived from its governing differential equation 4.8.

$$[M]\{\ddot{U}\}+[C]\{\dot{U}\}+\{F\}= -[M]\{1\}\ddot{u}_g \qquad 4.8$$

where [M] is the mass matrix, [C] is the damping matrix, {F} is the story force vector, {1} is an influence vector characterizing the displacements of the masses when a unit ground displacement is statically applied and üg is the ground acceleration history.

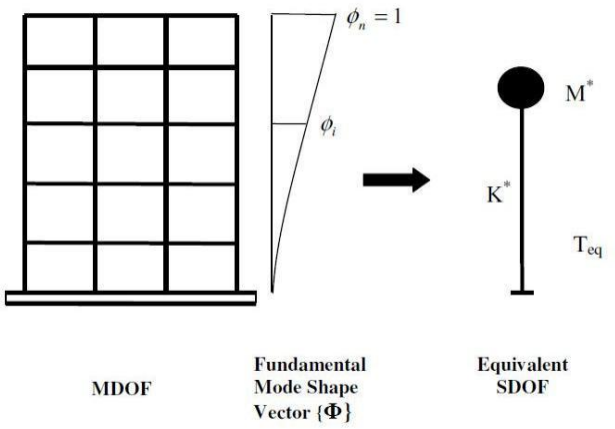

Figure 3-6: Conceptual transformation of MDOF to SDOF System

3.3.1 Non- Linear Plastic Hinge Properties

The building has to be modelled to carry out nonlinear static pushover analysis. This requires the development of the force - deformation curve for the critical sections of beams, columns. The force deformation curves in flexure were obtained from the reinforcement details and were assigned for all the beams and columns. The Nonlinear properties of beams and columns have been evaluated using the section designer and have been assigned to the computer model in SAP2000. The flexural default hinges (M3) and shear hinges (V2) were assigned to the beams at two ends. The interacting (P-M2-M3) frame hinges type a coupled hinge property was also assigned for all the columns at upper and lower ends.

The following equations are given in FEMA356: 2000 to calculate the yield moment and yield rotation of steel columns. The equation makes use length of member, cross sectional area, plastic modulus, moment of inertia and modulus of elasticity for the calculation of yield moment and yield rotation.

For Columns:

Yield rotation

$$\theta_y = {ZF_{ye}L_C\left(1-\frac{P}{P_{ye}}\right)}\Big/{(6EI_b)} \qquad 4.9$$

Yield Moment

$$M_y = 1.18\, ZF_{ye}\left(1 - \frac{P}{P_{ye}}\right) \leq Z.F_{ye} \qquad 4.10$$

Where

Z = plastic section modulus

F_{ye} = expected yeild strength

L_C= length of member along which deformations are assumed to occur

P=axial force in a member

P_{ye} =expected yield axial strength of a member

E=young's modulus of elasticity

I_b= moment of inertia of a beam

Table 3-4 Force Deformation Table

	Moment/yield moment	Rotation/SF
A	0	0
B	1	1
C	1.27	9
D	0.6	9.09
E	0.6	11

The force deformation relation based on Equations 4.9-4.10 and Table 3-4 is illustrated in Figure 3-7

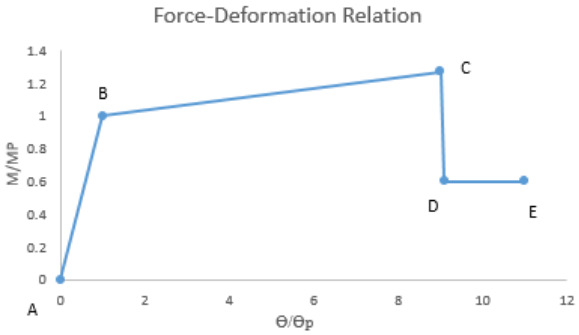

Figure 3-7: Force Deformation Relation

3.4 Capacity Spectrum Method

The building performance level can be determined by target displacement using the capacity spectrum method (ATC40). The capacity spectrum method allows for a graphical comparison between the structure capacity and the seismic demand. The pushover curve represents the lateral resisting capacity and the response spectrum curve represents the seismic demand.

The capacity spectrum method, which is described in Figure 3-8, is first started producing a force- displacement curve that considers the inelastic condition. The result is then plotted to ADRS (Acceleration Displacement Response Spectrum). The demand is also converted into ADRS format so that the capacity and the demand curve are in same format.

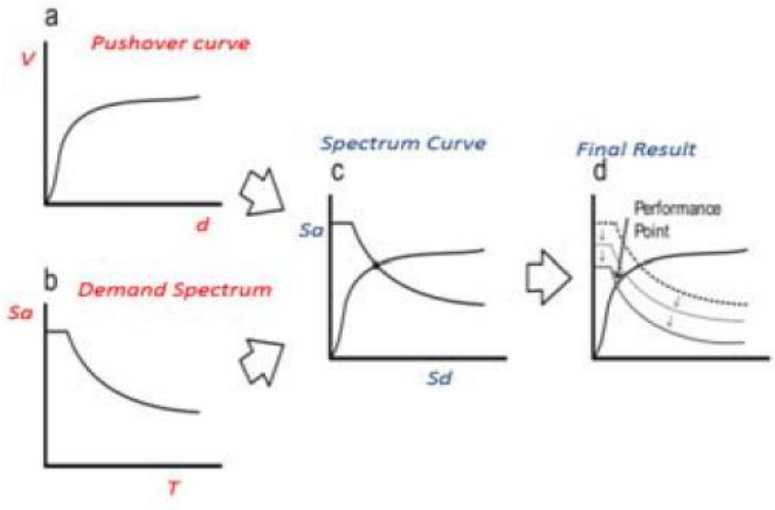

Figure 3-8 Capacity Spectrum Method

The response spectra used in thesis is NBC105 (2020) which is given in Figure 3-9.

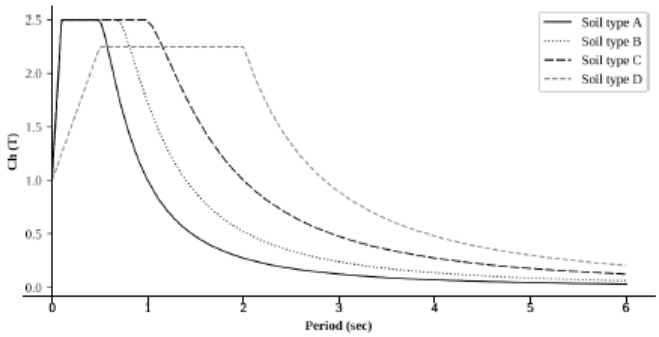

Figure 3-9: Response Spectrum of NBC 105(2020) for Non Linear Analysis

The general process for converting the capacity curve to capacity spectrum is to first calculate the modal participation factor (MPF1) and the modal mass coefficient (α), using the following equations:

$$\mathrm{MRF}_1 = \frac{\sum m_i \emptyset_{i1}}{\sum m_i \emptyset_{i1}^2} \quad 4.11$$

$$a = \frac{[\sum m_i \emptyset_{i1}]^2}{\left[\sum_{i=1}^{N} \frac{w_i}{g}\right]\left[\sum_{i=1}^{N} m_i {\emptyset_{i1}}^2\right]} \quad 4.12$$

Where:

$\frac{w_i}{g}$= mass assigned to level i

$\emptyset_{i1}$=amplitude of mode 1 at level i

N = level N

Then S_a and S_d are calculated for every point on the capacity curve using the following equations:

$$\frac{S_a}{g} = \frac{V_a}{w} . \frac{1}{a} \quad 4.14$$

$$S_d = \frac{\Delta_{roof}}{\mathrm{MPF}_1 \emptyset_{roof}} \quad 4.15$$

Where:

V= base shear

W=building load weight

Δ_{roof} = roof displacement

To convert a demand spectrum from S_a and T format to ADRS format, it is required to calculate the value of S_d for each point of the curve using the following equation:

$$S_d = \frac{T^2 S_a}{4\pi^2} \quad 4.15$$

The performance point is obtained by superimposing demand spectrum on capacity curve into spectral coordinate or ADRS format. The capacity spectrum method has been built in SAP2000 program.

3.5 Fragility Curve

Fragility Function

Fragility function as a mathematical function that expresses the probability that some undesirable event occurs (typically that an asset a facility or a component reaches or exceeds some clearly defined limit state) as a function of some measure of environmental excitation (typically a measure of acceleration, deformation, or force in an earthquake, hurricane, or other extreme loading condition).

Fragility function represents the cumulative distribution function of the capacity of an asset to resist an undesirable limit state.

Here, "cumulative distribution function" means the probability that an uncertain quantity will be less than or equal to a given value, as a function of that value.

Methodology for fragility curve generation

In this study, the author uses the methodology proposed by Wen et al. (2004) for the generation of fragility curves. The probability that the given structure exceeds the limit damage state for given ground motion intensity is provided by:

$$P(LS_I/GMI) = 1 - \emptyset\left(\frac{\lambda_{CL-}^{i} - \lambda_{D/GMI}}{\beta_{D/GMI}}\right) \quad 4.16$$

where,

$P(LS_I/GMI)$ is the probability of exceeding a particular limit state given ground motion intensity(GMI)

The limit state of damage used in this thesis is defined in the Table 3-5

Table 3-5: Inter Story Drift of Damage State defined in FEMA (2003) HAZUS

Inter Story Drift at Threshold of Damage State			
Slight	Moderate	Extensive	Collapse
0.004	0.0069	0.0157	0.04

φ(.) is the standard normal cumulative distribution function

λ_{CL}^{i} is ln(median story drift for a particular limit state, i

λ_D/GMI is ln(calculated median demand story drift given the GMI from the best fit power-law line)

β_D/GMI is the demand intensity

The two parameters λ_D/GMI and β_D/GMI are given by:

$$\lambda_D/GMI = lna_1 + a_2 \ln(GMI) \tag{4.17}$$

$$\beta_D/GMI = \sqrt{\frac{\sum_{k=1}^{n}[LN(GMI_k) - \lambda_D/GMI\,(GMI_k)]^2}{n-2}} \tag{4.18}$$

The constants a_1 and a_2 are obtained through linear regression analysis which is obtained by plotting (log-log form) natural logarithmic values corresponding to story drift and PGA (which is the GMI) . β_D/GMI is the square root of the standard error of the data, where *n* is the number of data points.

CHAPTER-4 CASE STUDY ON A PROTOYPE RESIDENTIAL STEEL BUILDING

4.1 Modelling and Analysis of the Structure

4.1.1 General

In this chapter, we discuss the modeling of the structural members and the loads applied to the structure. In general, the beams and columns are modeled as steel frame elements and the soil as the link elements. Finite element analysis software SAP2000v22.0.2 “Integrated software for analysis and design” is used for both linear and nonlinear analysis.

4.1.2 Structural Modelling

The steel framing systems considering SSI are modeled for analysis. The frame system consists of two and half story, three and half story, four and half story and five and half story buildings.

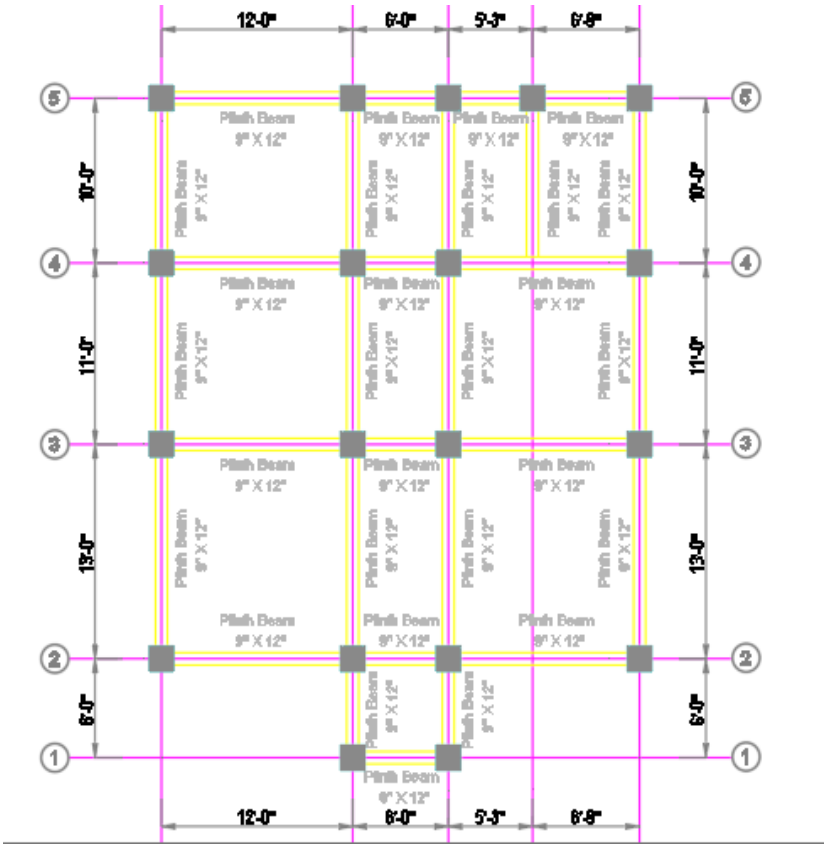

Figure 4-1 Floor Plan

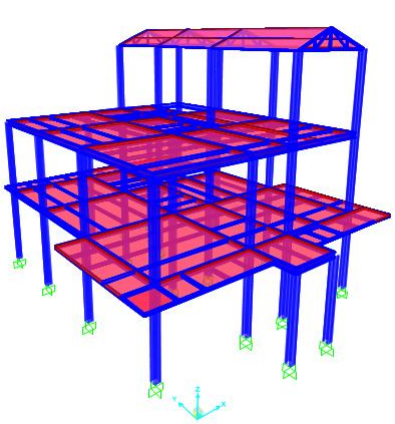

Two and Half Story Building

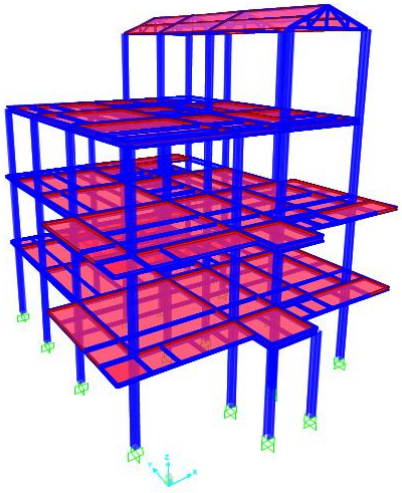

Three and Half Story Building

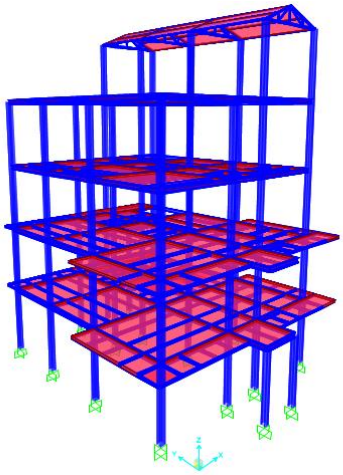

Four and Half Story Building

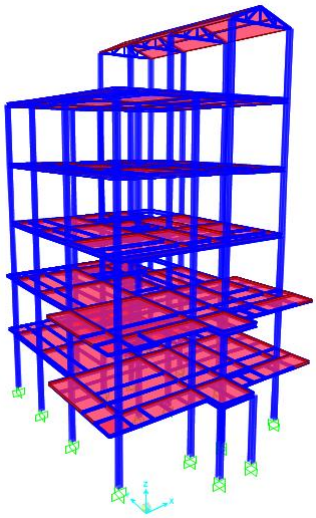

Five and Half Story Building

Figure 4-2 3D Model for the Steel Building prototypes

4.1.3 Material Properties

Fe250 grade steel is used for all the beams and columns in this study. The weight per unit volume is assumed to be 76.97 kN/m^3 with the Modulus of elasticity to be 210 GPa and Poisson ratio as 0.3. The minimum yield stress is taken as 250 MPa and minimum tensile stress is taken as 410 MPa.

4.1.4 Structural Elements

The structural elements resist the lateral loads through bending of steel beams and bending as well as axial deformation of columns. The behavior of the structure is dependent upon the beam-column connections. In this study, the beam-column connection is assumed to be a moment-resisting connection, i.e. the connection can transfer moments from beam to columns and vice versa.

The beam and column members used for analysis are shown in Table 4-1.

Table 4-1 Beam and Column Members

No of Story	Beam	Column
1	ISMB 200	2ISMC250
2	ISMB 200	2ISMC250
3	ISMB 200	ISB91.5*91.5

Table 4-2: Element Unit Weight from IS 800:1989

Element	Unit weight	unit
2ISMC 250	68.4	kg/m
ISMB200	24.2	kg/m
ISMB100	8.9	kg/m
ISB49.5X49.5X2.9	3.66	kg/m
ISB72*72*4	8.22	kg/m

The seismic weight of the building calculated is shown in the table below:

Table 4-3: Seismic Weight of the Steel Building for Different Story

2 and half		3 and half		4 and half		5and half	
Story level	Seismic wt. (kN)	Story level	Seismic wt. (kN)	Story level	Seismic wt. (kN)	Story level	Seismic wt. (kN)
						6	30.65
				5	30.65	5	507.95
		4	30.65	4	507.95	4	675.513
3	30.65	3	507.95	3	675.513	3	675.513
2	507.95	2	675.51	2	675.513	2	675.513
1	675.51	1	675.51	1	675.513	1	675.513
Total	1183.46	Total	1889.62	Total	2565.14	Total	3240.65

4.1.5 Soil Idealization

The structure is assumed to be supported by firm non liquefiable soil produced by inertia of structure. The present study considers translations of foundations in two mutually perpendicular principal horizontal directions and vertical direction as well as rotations of the same about these three directions. For the buildings with the raft foundation, the link supports have been attached below the column to simulate the effect of soil flexibility taking three translational two along horizontal and one vertical axes together with three rotation about these three mutually perpendicular axes. The stiffness and damping of this centrally placed link for raft type is based on Gazetas (1991).

The value of the stiffness and the damping for the individual column in all considered degree of freedom is approximated by considering the tributary area of the individual column in raft. To obtain the values of the stiffness of the springs for soil, value of shear modulus (G) of the soil have been estimated using the shear wave velocity.

The other details of soil parameters are tabulated in table:

Table 4-4 Soil Parameters Chhetri and Thapa(2015)

Shear wave velocity (v_s) (m/s)	Poisson's ratio (μ)	Unit weight (ρ) (kN/m^3)
100	0.3	16

Foundation value

The value of the dimensions used in the building prototype are shown in Table 4-5.

Table 4-5 Foundation Dimensions for Prototype building

L(m)	B(m)	D(m)	I_{bx}(m^3)	I_{by}(m^3)	J_b(m^3)
6.06	4.49	0.5	581.27	554.87	1136.14

Table 4-6 Foundation properties of Prototype building

G	χ	a_0	μ	A_b	A_w	w(omega)
16400000	0.74	0.41	0.3	109.03	8.99	9.30

Table 4-7 Values calculated for the Prototype

T(1)	ρ	v_s	v_{la}
0.67	1640	100	154.68

Table 4-8 Dynamic property obtained from graph Figure 3-2

c_z	c_y	c_z	c_{rx}	c_{ry}	c_{rz}
1	0.9	0.5	0.1	0.12	0.1

The distribution factor obtained for the spring stiffness is given below:

The total stiffness and the damping of the spring where distributed based on the area of the individual column occupied.

Table 4-9 Distribution factor

Column IDs	Area (m^2)	Distribution factor (d-factor)
1	2.78	0.028874
2	5.85	0.060635
3	6.68	0.069298
4	3.62	0.037537
5	4.180637	0.04331
6	8.779337	0.090952
7	10.03367	0.103947
8	6.271092	0.064967
9	0.836127	0.008662
10	2.612898	0.027069
11	8.047726	0.083373
12	9.197527	0.095284
13	5.818179	0.060275
14	0.836127	0.008662
15	2.670962	0.027671
16	1.45161	0.015038
17	6.096762	0.063161
18	6.967823	0.072185
19	3.774281	0.039101
Total	96.52716	1

The plan for the distribution and the column numbering shown in Figure 4-3 below:

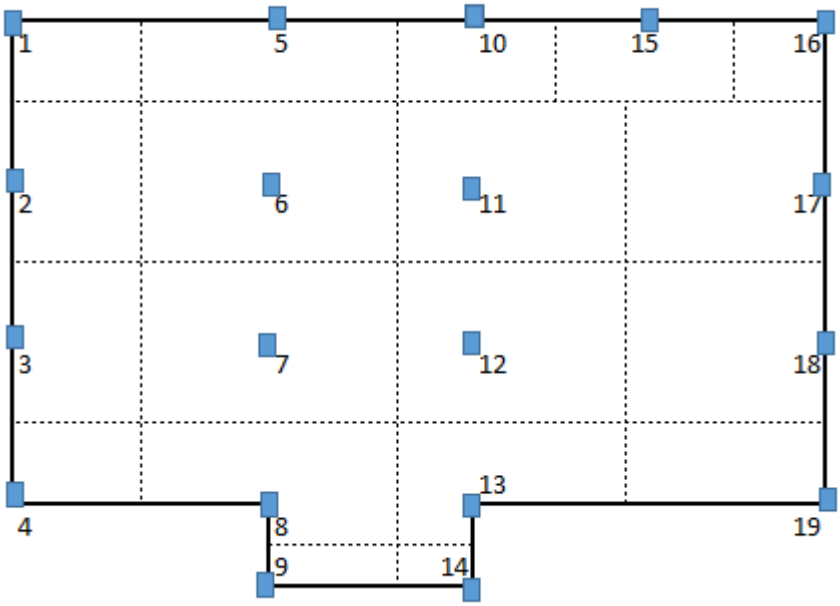

Figure 4-3 Plan for Distribution Factor and Column Numbering

The total dynamic stiffness value is given in Table 4-10 and individual dynamic stiffness can be obtained for different column of the building are as shown below in Table 4-11. Similar values for the other building cases can be found in Annex B. The illustration to calculate the total dynamic stiffness can be found in Annex C.

Table 4-10 Total Dynamic Stiffness value of the building (two and half story)

Total Dynamic Stiffness of the Building (kN/m)					
k_z	k_y	k_x	k_{xx}	k_{yy}	k_{zz}
540281.3	442335.5	431369.3	7588514.4	7161645.7	11512505.8

Table 4-11 Dynamic Stiffness for the Individual Column (two and half story)

Column	d-factor	Dynamic Stiffness for Individual Column (kN/m)					
		k_z	k_y	k_x	k_{xx}	k_{yy}	k_{zz}
1	0.029	15599.9	12771.8	12455.2	219108.1	206782.8	332408.0
2	0.061	32759.8	26820.9	26155.9	460127.0	434244.0	698056.9
3	0.069	37440.3	30652.8	29892.9	525866.6	496285.6	797790.2
4	0.038	20280.4	16603.8	16192.2	284847.7	268824.5	432141.4
5	0.043	23399.8	19157.8	18682.8	328662.1	310174.3	498612.1
6	0.091	49139.7	40231.3	39233.9	690190.5	651365.9	1047085.3
7	0.104	56160.4	45979.3	44839.4	788799.9	744428.4	1196685.3
8	0.065	35100.5	28737.3	28024.8	493004.0	465271.6	747934.5
9	0.009	4680.0	3831.6	3736.6	65732.4	62034.9	99722.4
10	0.027	14624.9	11973.6	11676.8	205413.8	193858.9	311632.5
11	0.083	45044.7	36878.7	35964.4	632674.6	597085.4	959828.2
12	0.095	51480.3	42147.7	41102.7	723066.6	682392.7	1096961.5
13	0.060	32565.5	26661.8	26000.8	457398.0	431668.5	693916.8
14	0.009	4680.0	3831.6	3736.6	65732.4	62034.9	99722.4
15	0.028	14949.9	12239.7	11936.2	209978.6	198166.9	318557.7
16	0.015	8124.9	6652.0	6487.1	114118.8	107699.4	173129.2
17	0.063	34124.8	27938.4	27245.8	479299.0	452337.5	727142.6
18	0.072	39000.3	31930.0	31138.4	547777.7	516964.2	831031.5
19	0.039	21125.4	17295.6	16866.9	296716.4	280025.5	450147.3
Sum	1						

The total damping value is given in Table 4-12 and the dynamic damping is obtained for individual columns of the building are as shown below in Table 4-13. Similar values for the other building cases can be found in Annex B.

Table 4-12: Total Damping Value of the building (two and half story)

Total Damping ($kNsm^{-1}$)					
c_z	c_y	c_x	c_{xx}	c_{yy}	c_{zz}
27659.8	16093.1	17881.3	14746.0	16891.7	18632.8

Table 4-13 Individual Damping Value for Individual Column (two and half story)

Column	d-factor	Individual Damping value for individual column ($kNsm^{-1}$)					
		c_z	c_y	c_x	c_{xx}	c_{yy}	c_{zz}
1	0.029	798.6	464.7	516.3	425.8	487.7	538.0
2	0.061	1677.1	975.8	1084.2	894.1	1024.2	1129.8
3	0.069	1916.8	1115.2	1239.1	1021.9	1170.6	1291.2
4	0.038	1038.3	604.1	671.2	553.5	634.1	699.4
5	0.043	1198.0	697.0	774.4	638.7	731.6	807.0
6	0.091	2515.7	1463.7	1626.3	1341.2	1536.3	1694.7
7	0.104	2875.1	1672.8	1858.7	1532.8	1755.8	1936.8
8	0.065	1797.0	1045.5	1161.7	958.0	1097.4	1210.5
9	0.009	239.6	139.4	154.9	127.7	146.3	161.4
10	0.027	748.7	435.6	484.0	399.2	457.2	504.4
11	0.083	2306.1	1341.7	1490.8	1229.4	1408.3	1553.5
12	0.095	2635.5	1533.4	1703.8	1405.1	1609.5	1775.4
13	0.060	1667.2	970.0	1077.8	888.8	1018.1	1123.1
14	0.009	239.6	139.4	154.9	127.7	146.3	161.4
15	0.028	765.4	445.3	494.8	408.0	467.4	515.6
16	0.015	416.0	242.0	268.9	221.8	254.0	280.2
17	0.063	1747.0	1016.5	1129.4	931.4	1066.9	1176.9
18	0.072	1996.6	1161.7	1290.8	1064.4	1219.3	1345.0
19	0.039	1081.5	629.3	699.2	576.6	660.5	728.6
sum	1						

4.1.6 Loading

Besides the self–weights of the sections, the following loads were applied to the models, floor finish of $2.5kN/m^2$, live load of $1.25kN/m^2$ and wall load of 1kN/m.

CHAPTER-5 RESULT AND DISCUSSION

5.1 Modal Analysis

Modal analysis is carried out in CSI SAP2000 V22 for steel building of two and half story, three and half story, four and half story and five and half story in fixed base and flexible base condition. The fundamental time period for fixed base condition and for flexible base condition are as shown in Table 5-1. The time periods for SSI base buildings are comparatively higher than the fixed base buildings.

Table 5-1 Fundamental Time Period for Fixed and SSI

No of story	Time period for fixed case (sec)	Time period for SSI case (sec)
Two and half	0.372	0.510
Three and half	0.585	0.646
Four and half	0.767	0.847
Five and half	1.080	1.287

Table 5-2 and Table 5-3 show the natural time periods and modal participation ratios of first twelve modes respectively for fixed base and flexible base conditions. From Table 5-2 and Table 5-3it is clear that as the height of the building increases, the higher modes participation comes into effect in both fixed and SSI.

Table 5-2: Modal Mass Participation Ratio of the Building with Fixed Base Footing

Cases	Two And Half				Three and Half				Four and half				Five and half			
Mode No	Period	UX	UY	RZ	Period	UX	UY	RZ	Period	UX	UY	RZ	Period	UX	UY	UZ
1*	0.372	0.0001	0.861	0.000	0.586	0.0005	0.830	0.000653	0.768	0.000582	0.8	0.00154	1.086	0.0004	0.78	0.002304
2	0.359	0.8355	0.0001	0.031	0.560	0.6700	0.00088	0.16	0.721	0.73	0.001106	0.07182	1.019	0.7200	0.00121	0.06722
3	0.318	0.0394	0.0001	0.829	0.504	0.1700	0.00008	0.67	0.649	0.08157	0.000572	0.71	0.916	0.0775	0.00207	0.69
4	0.223	0.0007	0.0005	0.0000	0.224	0.0006	0.00085	0.00003	0.259	0.004227	0.12	0.00392	0.384	0.0064	0.12	0.009318
5	0.144	0.0005	0.0001	0.0004	0.223	0.0001	0.00005	1.3E-07	0.257	0.08234	0.007407	0.04132	0.375	0.0904	0.01251	0.03399
6	0.131	0.0868	0.0004	0.0559	0.189	0.0001	0.13000	0.000004	0.234	0.03793	0.000028	0.09303	0.344	0.0341	0.00107	0.11
7	0.125	0.0004	0.1346	0.0006	0.186	0.0856	0.00003	0.03504	0.224	0.000025	0.000006	0.00011	0.275	0.0001	0.00013	0.000008
8	0.112	0.0345	0.0000	0.0787	0.170	0.0272	0.00008	0.08574	0.223	0.001163	0.00053	0.00015	0.274	0.0002	0.00014	1.62E-07
9	0.092	0.0000	0.0000	0.0008	0.144	0.0004	0.00006	0.00021	0.145	0.002782	0.000827	0.00151	0.208	0.0002	0.05032	0.000445
10	0.087	0.0000	0.0000	0.0001	0.144	0.0002	0.00002	0.00009	0.144	0.000657	0.000089	0.00041	0.204	0.0396	0.00056	0.01011
11	0.074	0.0015	0.0000	0.0000	0.116	0.0251	0.00011	0.02088	0.138	0.01451	0.02842	0.00923	0.185	0.0051	0.00035	0.04117
12	0.073	0.0001	0.0017	0.0001	0.109	0.0003	0.038	0.00022	0.137	0.02397	0.02312	0.00942	0.177	0.0003	0.000078	0.00055
Total		0.999	0.999	0.998		0.980	1.00	0.973		0.980	0.982	0.942		0.974	0.968	0.965

* The first mode is the fundamental mode for the building.

Table 5-3: Modal Mass Participation Ratio of the Building for Flexible Base Footing

Cases	Two And Half				Three and Half				Four and half				Five and half			
Mode No	Period	UX	UY	RZ	Period	UX	UY	RZ	Period	UX	UY	RZ	Period	UX	UY	UZ
1*	0.510	0.1600	0.6800	0.0350	0.646	0.000003	0.83000	0.00093	0.848	0.0002	0.8000	0.0013	1.287	0.00177	0.780000	0.0003
2	0.506	0.6600	0.1800	0.0358	0.638	0.750000	0.00004	0.09892	0.825	0.7800	0.0001	0.0339	1.257	0.76000	0.001589	0.0290
3	0.426	0.0665	0.0059	0.8300	0.548	0.100000	0.00071	0.75000	0.695	0.0352	0.0011	0.7800	1.032	0.03005	0.000395	0.7600
4	0.328	0.0035	0.0029	0.0001	0.248	0.003906	0.00325	0.00022	0.276	0.0718	0.0422	0.0244	0.429	0.01634	0.120000	0.0059
5	0.217	0.0047	0.0012	0.0018	0.224	0.000705	0.00101	0.00007	0.274	0.0315	0.0968	0.0082	0.428	0.09857	0.023380	0.0303
6	0.175	0.0679	0.0018	0.0252	0.204	0.065210	0.03873	0.01574	0.247	0.0125	0.0000	0.0451	0.380	0.03756	0.000127	0.1100
7	0.167	0.0033	0.1100	0.0000	0.202	0.026340	0.08439	0.00733	0.245	0.0221	0.0001	0.0525	0.340	0.00003	0.000074	0.0000
8	0.157	0.0005	0.0017	0.0134	0.181	0.023430	0.00002	0.08669	0.224	0.0003	0.0001	0.0000	0.311	0.00002	0.000003	0.0000
9	0.146	0.0235	0.0012	0.0522	0.169	0.000643	0.00072	0.00021	0.172	0.0004	0.0000	0.0003	0.237	0.00124	0.000002	0.0008
10	0.137	0.0008	0.0002	0.0012	0.145	0.000237	0.00005	0.00012	0.150	0.0002	0.0000	0.0003	0.228	0.01149	0.025100	0.0049
11	0.133	0.0000	0.0006	0.0001	0.137	0.000028	0.00002	0.00006	0.147	0.0218	0.0018	0.0131	0.226	0.01798	0.017640	0.0050
12	0.130	0.0002	0.0000	0.0006	0.134	0.000006	0.00006	0.00000	0.144	0.0036	0.0006	0.0022	0.207	0.00000	0.000736	0.0013
Total		0.9909	0.9855	0.9953		0.97050	0.9589	0.96028		0.9795	0.9427	0.9613		0.9750	0.9690	0.947
* The first mode is the fundamental time period of the building.																

5.2 Pushover Analysis

The pushover analysis is performed for each of two and half story, three and half story, four and half story and five and half story building to find the capacity of the building. The nonlinear behavior is characterized by assigning plastic hinge in frame staging elements. Column members are assigned with P-M2-M3 user defined hinged as defined in the section 3.3.1 and beam members are assigned with M3 auto hinge. The nonlinear analysis performed shows the different limit states and progression of plastic hinges as shown in Figure 5-1. As a representative example, the plastic hinges formed at different pushover steps for two and half story building is illustrated in Figure 5-1, where plastic hinge initiated from the ground story columns and progressively moved upwards. It should be noted that similar observations of progression of plastic hinges were also made for other building types considered in this work. Figure 5-4 and Figure 5-5 show the pushover curves for all the buildings.

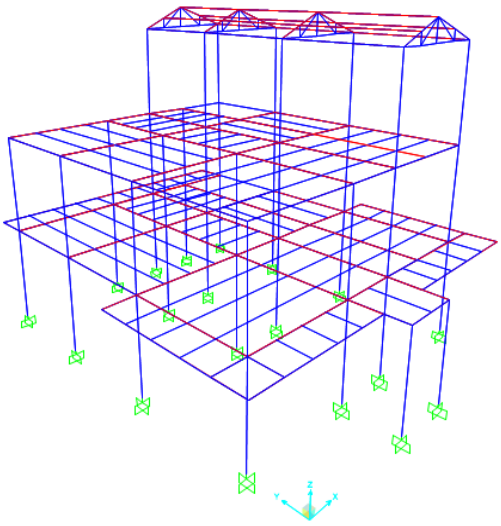

Step 1 for two and half story for Fixed case

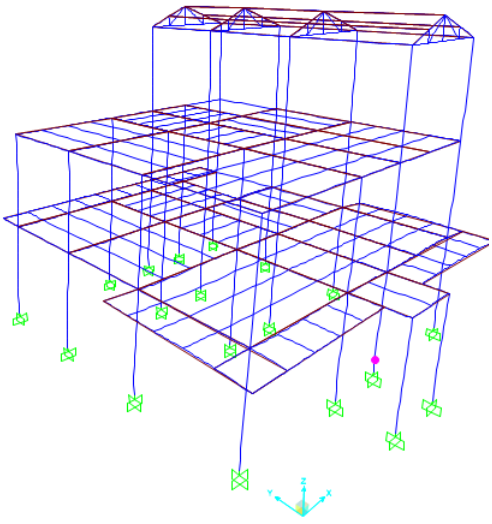

Step 67 for two and half story for Fixed case

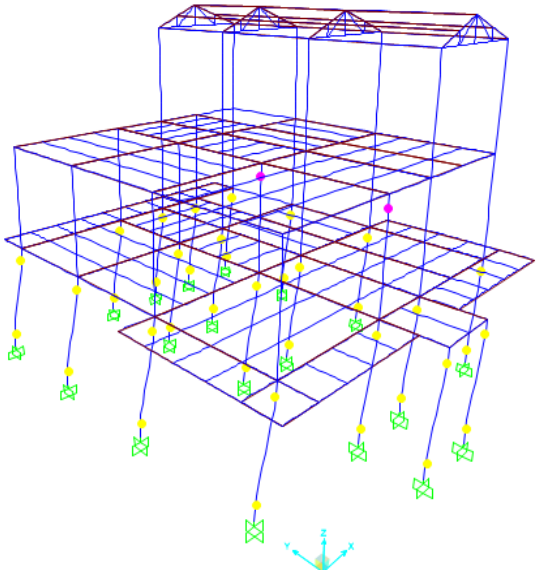

Step 292 for two and half story for Fixed case

Figure 5-1: Progression of Hinges Formation for Different Limit States in Pushover Analysis

Figure 5-2 and Figure 5-3 show the progression of story drifts for each building type as the building is pushed during the pushover analysis. The results for selective load steps are only presented for brevity. Initially, the building is in linear range as shown in Figure 5-2 and Figure 5-3 with linear distribution of drifts along the height of the building. As the building is further pushed, differentiation in story drift was observed with formation of plastic hinges. Figure 5-1 clearly shows that the plastic hinge formation started from the ground story columns which can also be verified from Figure 5-2 and Figure 5-3, where significantly large story drift was found at the first story level for all the building models adopted in both the fixed and SSI case. Therefore, to interpret the pushover curve, capacity of building and identify the limit states in the next section, drift of first story is chosen.

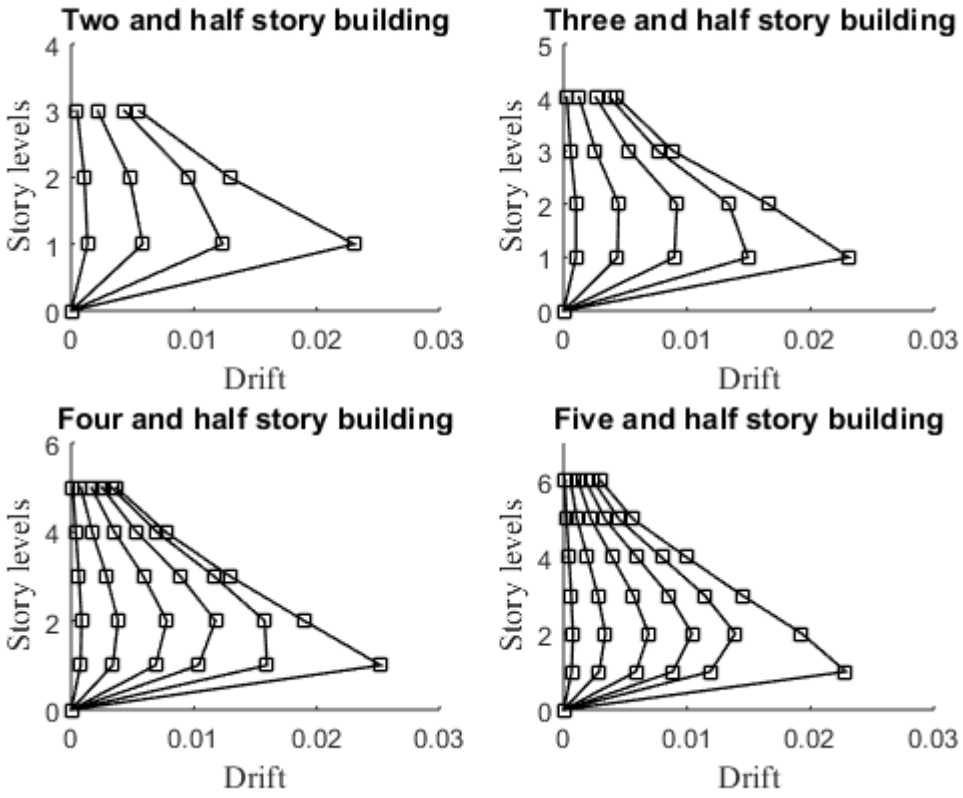

Figure 5-2: Progression of Drift for Selective Pushover Steps for Fixed base

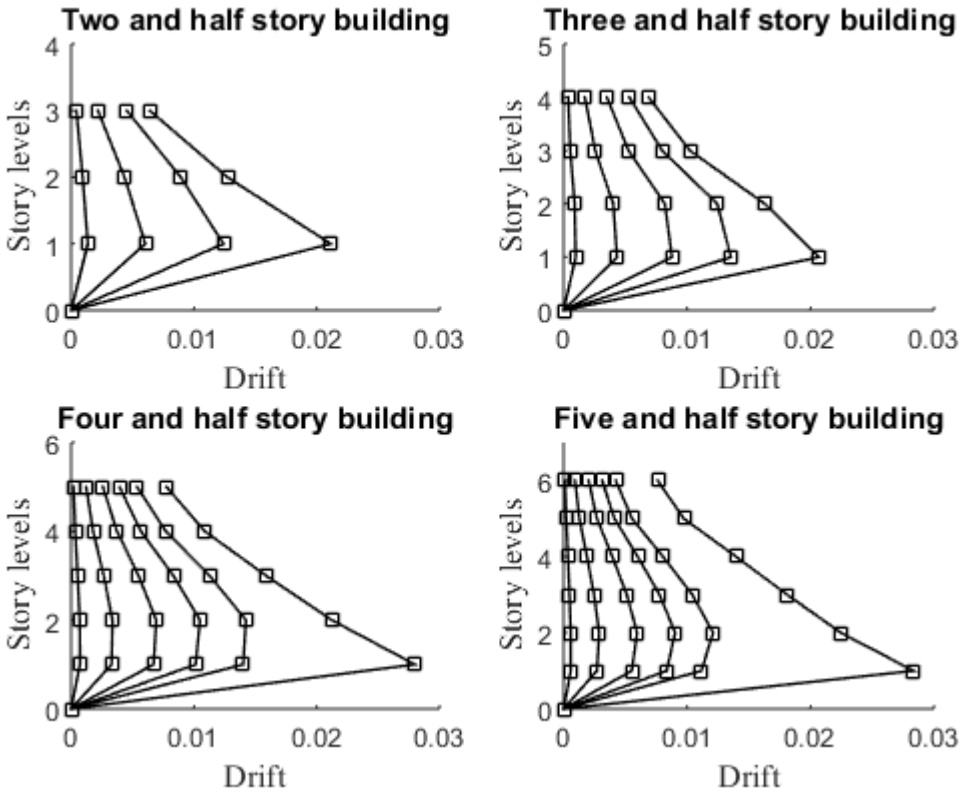

Figure 5-3: Progression of Drift for Selective Pushover Steps for SSI base

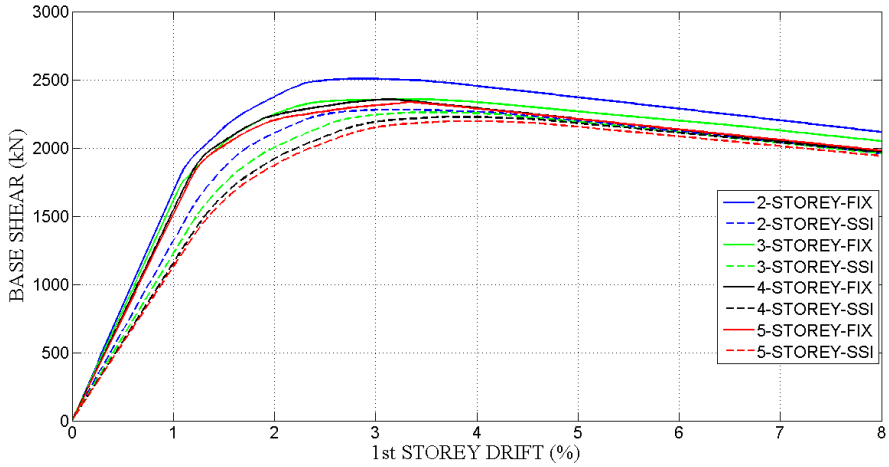

Figure 5-4: Pushover Analysis Result of Base Shear for 1st Story Drift

Figure 5-4 shows the pushover curves for the all the buldings considered with respect to the 1st story drift. The maximum drift is 8% and the maximum base shear is 2500kN. For the same story building the base shear for fixed base is greater than SSI case. Further with the changes in the story levels, two and half story building has base shear greater than the three and half, four and half and five and half story buildings for both fixed and SSI case. The first plastic hinge is formed in the first story as shown in the Figure 5-1 which shows the movement of the structure from linear elastic range to nonlinear range hence, understandably, the first story drift is maximum for the buildings compared to the drifts of higher stories for all the buildings. From Figure 5-5, it shows that the maximum top story drift is 3% which is comparatively lower to 1st story drift in Figure 5-2.

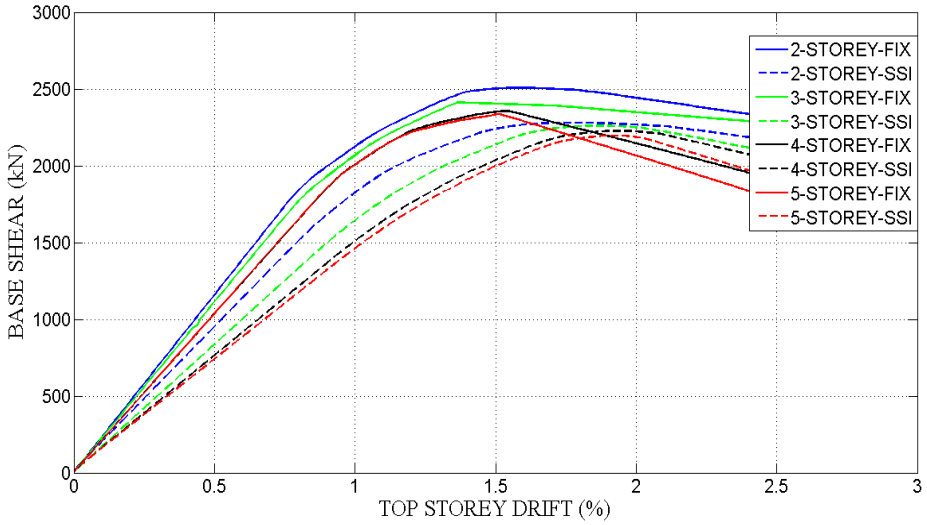

Figure 5-5: Pushover Analysis of Base Shear for Top Story Drift

5.3 Capacity Spectrum Method

After the pushover analysis, a structural performance point is obtained by intersecting the capacity curve with the demand from the response spectrum of NBC105 (2020) as described in Section 3.4 previously. As the structure is deformed beyond the elastic limit for nonlinear static analysis, the elastic demand is also reduced so as to incorporate the inelastic dissipation of the structure. Here, the response spectrum of the NBC 105(2020) is reduced to different ductility for the nonlinearity of the structure (hysteretic damping) as shown in Figure 5-6.

With determination of the performance point, spectral acceleration, base shear and drift is obtained as shown in Figure 5-6. The performance points for two and half story steel building for 0.1g, 0.4g, 0.6g and 1.0g for fixed base footing is shown in Figure 5-6. Similar procedures are followed for three and half, four and half and five and half story building for both fixed base and SSI case which are shown in detail in the Annex A.

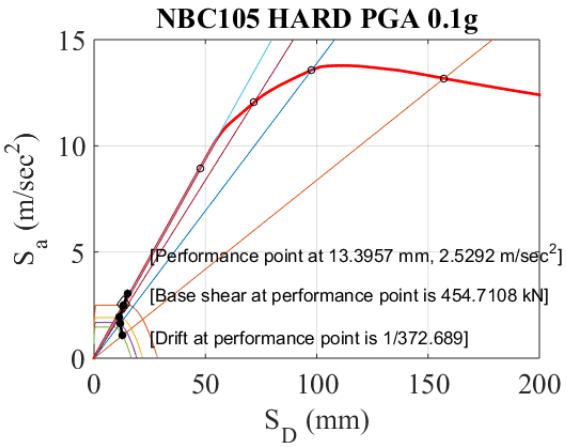

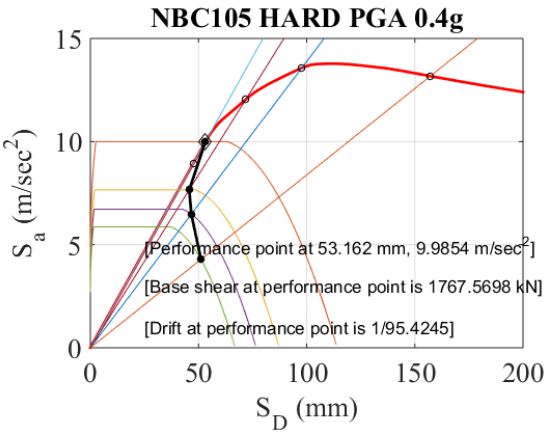

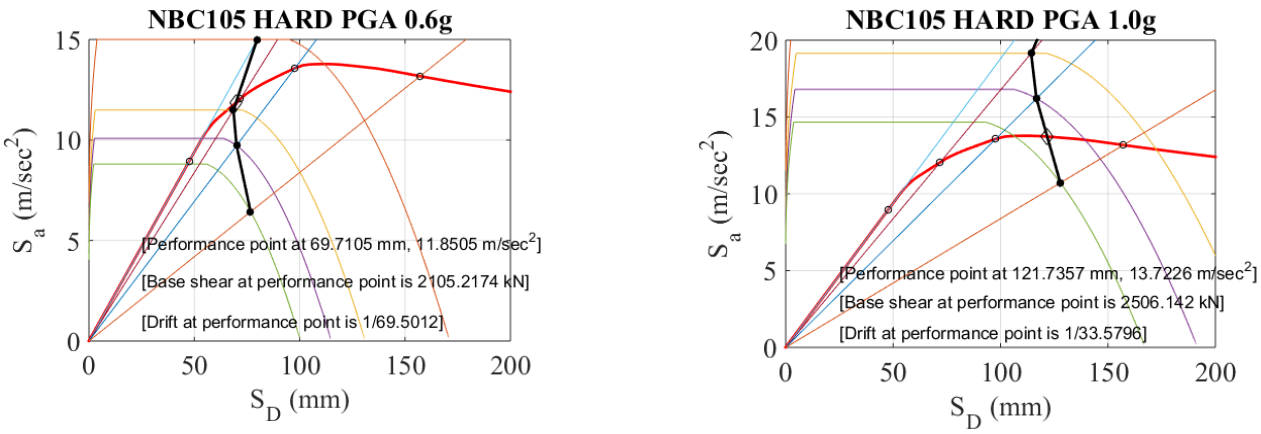

Figure 5-6: Performance Point for Different PGA for Two and Half Story Building

From Figure 5-7, the maximum base shear for two and half story, three and half story, four and half, five and half story for fixed case are 2506.14kN, 2466.50kN, 2303.43kN, 2236.28kN respectively. Similarly, the maximum base shear for SSI case counterparts are 2279.28kN, 2183.63kN, 1196.10kN, 1828.79kN respectively. With the increase of the height of the building, the base shear of the building decreases both for fixed case as well for SSI case. For the same height of the building, the base shear of the fixed case of the building is greater than SSI case.

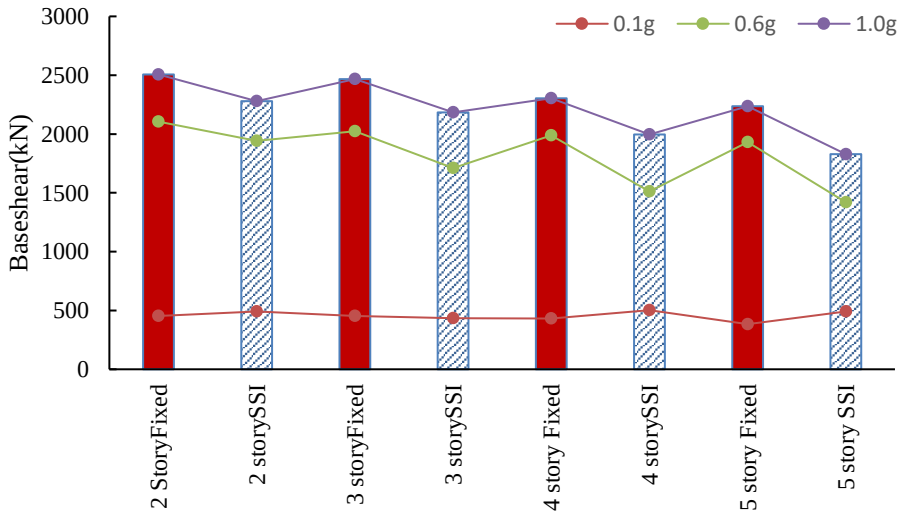

Figure 5-7: Variation of PGA with Story Height along with Base Shear

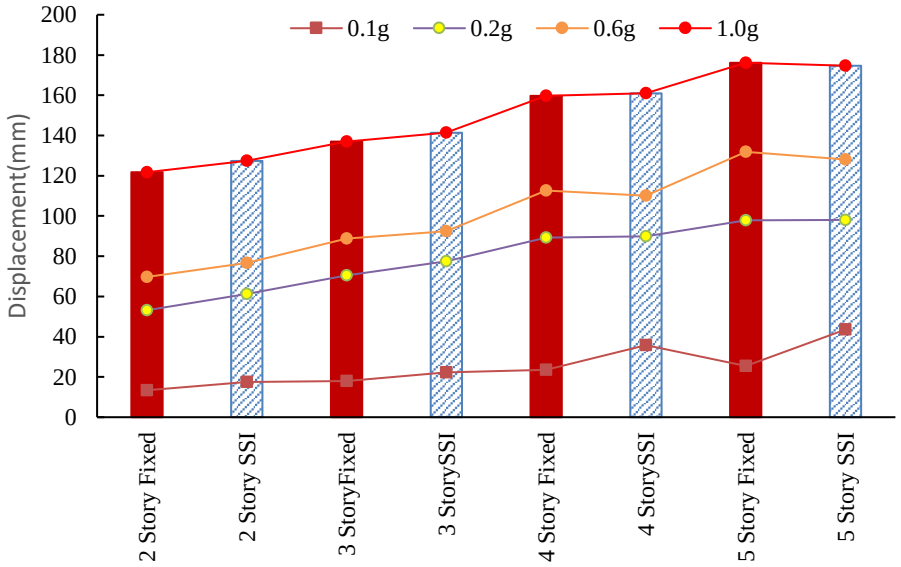

Figure 5-8: Variation of PGA with Story Height along with Displacement

Figure 5-8 shows the spectral displacements as obtained from the performance points for two and half, three and half, four and half and five and half story buildings for fixed case with their values 121.735mm, 136.977mm, 159.702mm, 176.136mm respectively. Similarly, for SSI case, the values are 127.347mm, 141.350mm, 160.923mm, and 174.656mm respectively. With increase of the height of the building the spectral displacements also increase and SSI case buildings have higher displacements for the same story building as compared to their fixed base counterparts.

5.4 Regression Analysis

For the fragility curve generation, the correlation between drift and PGA must be determined. Figure 5-9 shows the plots for drifts observed over the increasing levels of PGAs. The response of the building under the increasing levels of NBC 105 response spectrum PGAs shows progressively increasing trends from 0.1g to 1.0g.

The results obtained from the performance point for different story from capacity spectrum method is used to obtain the value of $a1$ and $a2$ as stated in section 3.5. From Figure 5-10, for fixed case $a1$ is 0.8707 and $a2$ is 0.9436 and for SSI case $a1$ is 0.7959 and $a2$ is 0.759. The goodness-of-fit (R^2) of the fixed case is 0.985 and SSI case is 0.948, hence, the discreteness of results is relatively small, and that fitting results are satisfactory.

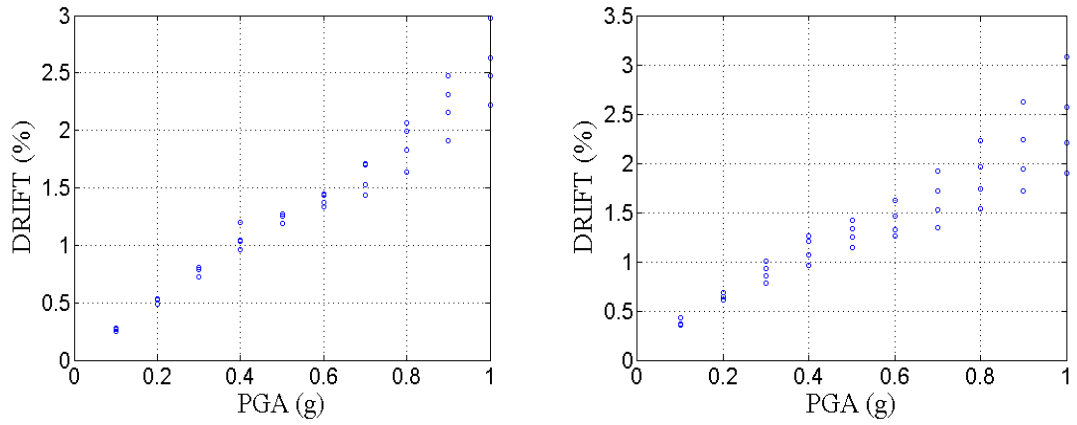

Fixed Base Case SSI Case

Figure 5-9: Distribution of Drift and PGA for Fixed base and SSI cases

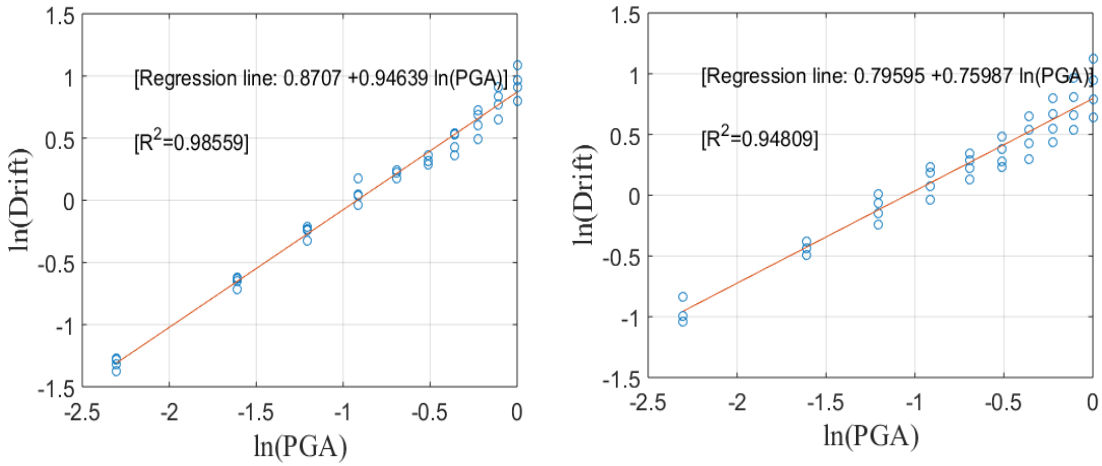

Fixed base Case SSI Case

Figure 5-10: Regression Analysis for Fixed and SSI case

5.5 Fragility functions

The analytical fragility curves are obtained from the fragility analysis. Fragility curve gives the conditional probability that the particular damage states exceeds the limiting value in given intensity parameter. In this study analytical fragility curves are obtained for both fixed base and SSI base conditions for the steel buildings considered. Wen et al. (2004) procedure is used to obtain the fragility curve for the system under consideration as described previously in Section 3.5. Figure 5-11, Figure 5-12, Figure 5-13, Figure 5-14 represents fragility curve for two and half story, three and half story, four and half story and five and half story building respectively.

Slight damage

For slight damage of two and half story building initially at 0.1g the probability of exceedance for SSI case is 0.4 and 0.3 for fixed case. The value of probability of exceedance of slight damage limit state for SSI case is more critical than the fixed base case up to 0.3g. Afterwards, the probability of exceedance for both fixed and SSI case remain almost the same for 0.4g and 0.5g. Similar observations were made for three and half, four and half story and five and half story buildings as well.

Moderate damage

For moderate damage of two and half story building initially at 0.1g probability of the exceedance for SSI is 0.35 while 0.3 for fixed case and similarly the value of exceedance for SSI is greater than fixed case up to o.4g. Afterwards, the probability of exceedance for both the fixed case and SSI case remain same for 0.5g. Similar observations were made for three and half, four and half story and five and half story buildings as well.

Extensive damage

For extensive damage of two and half story building initially at 0.1g probability of the exceedance for SSI is 0.1 while 0.075 for fixed case and similarly the value of exceedance for SSI is greater than fixed case up to 0.5g. However, the sensitivity and change in probability is relatively small for this limit state compared to the previous ones.

Complete damage

For complete damage of two and half story building initially at 0.1g probability of the exceedance for SSI is greater than fixed case and similarly the value of exceedance for SSI is greater than fixed case up to 0.5g. However, again, the change in probabilities of exceeding this limit state is relatively smaller compared to the previous limit states.

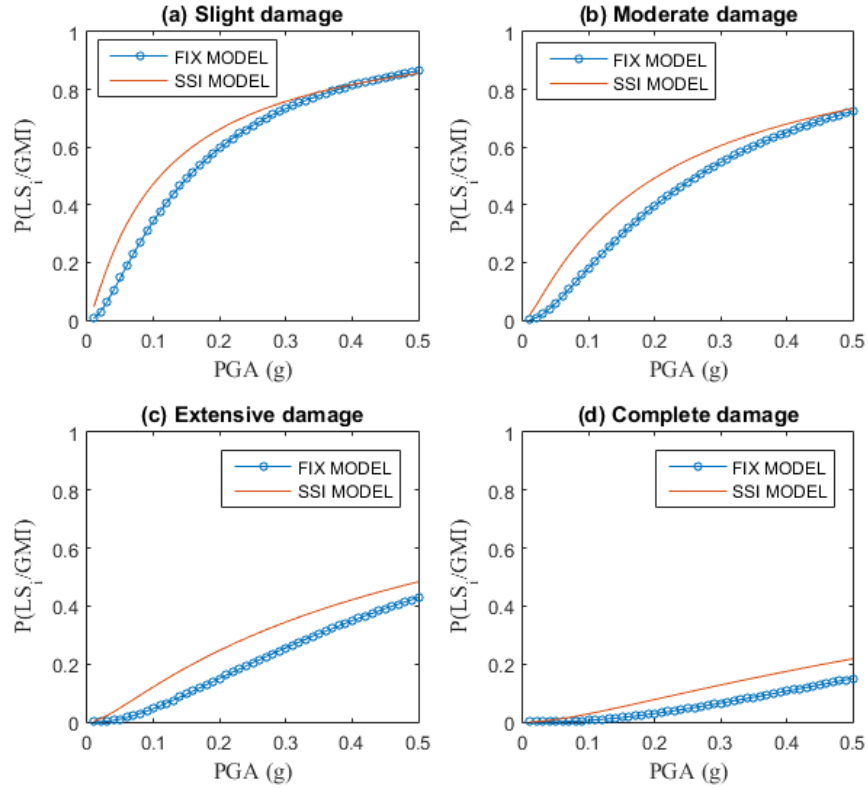

Figure 5-11: Fragility Curve for Two and Half Story Building

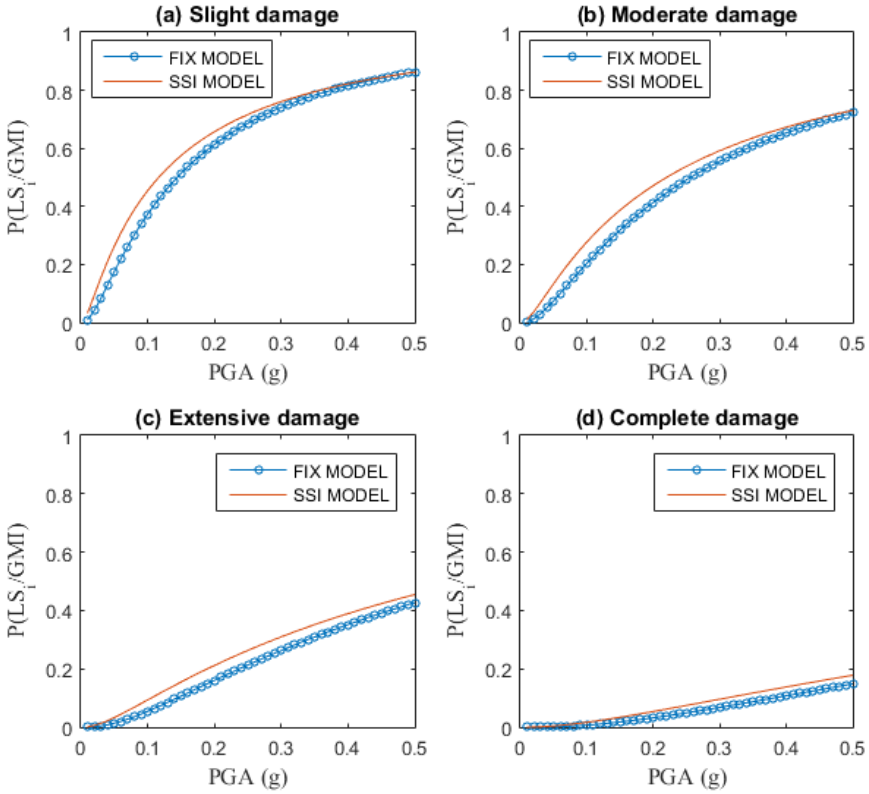

Figure 5-12: Fragility Curve for Three and Half Story Building

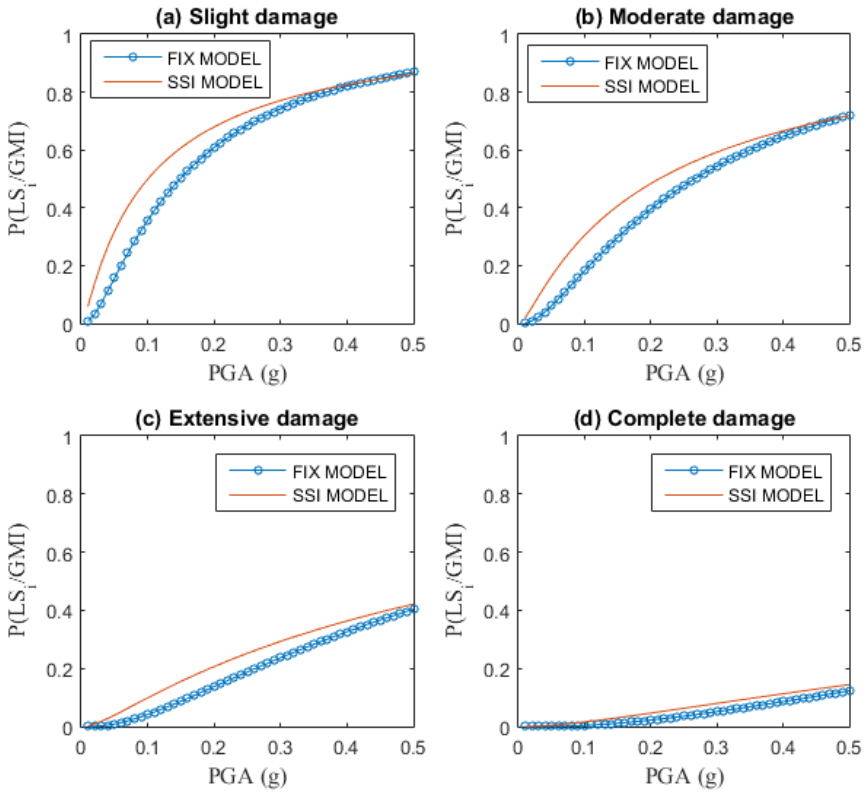

Figure 5-13: Fragility Curve of Four and Half Story Building

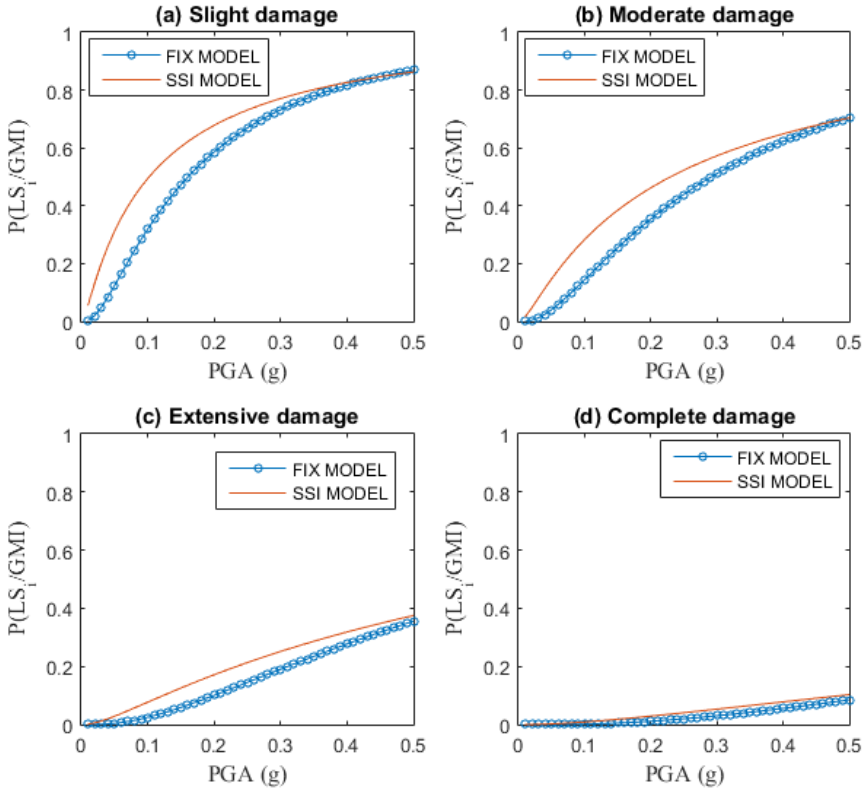

Figure 5-14: Fragility Curve of Five and Half Story Building

For ground motion beyond 0.5g and fragility curves considering all the four steel buildings is shown in Figure 5-15 and Figure 5-16. The fragility functions and probability of exceedance of respective limit states in Table 5-4 are described here for 0.2g, 0.6g and 1.0g representing minor level of shaking, moderate level of shaking and major level of shaking respectively.

Table 5-4: Probability of Failure for Residential Steel Building: Fixed Base Condition

PGA	Probability of reaching or exceeding damage states (%)			
	Slight damage	Moderate damage	Extensive damage	Complete damage
0.2	60	38	15	1
0.6	90	80	45	15
1.0	96	90	65	30

Table 5-5: Probability of Failure for Residential Steel Building SSI Base Condition

PGA	Probability of reaching or exceeding damage states (%)			
	Slight damage	Moderate damage	Extensive damage	Complete damage
0.2	70	45	20	2
0.6	85	78	46	18
1.0	95	85	62	28

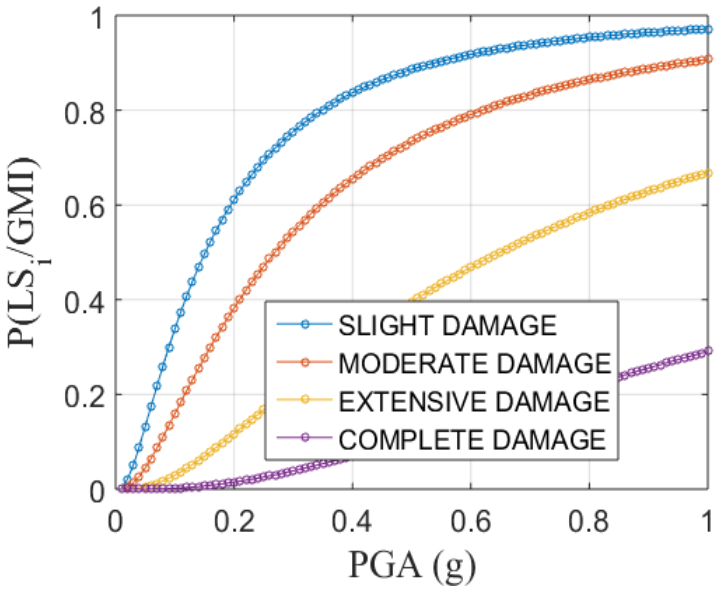

Figure 5-15: Fragility Curve for Fixed Case

For slight, moderate and extensive level of damage, the effect of SSI and flexibility of soil is found to be considerable whereas the effect is found minimum for complete damage limit state. The results show that the complete damage state is almost similar for both the fixed and SSI case. Furthermore, at lower PGAs the SSI case is more vulnerable than the fixed case but as the value of the PGAs increase the vulnerability is almost similar.

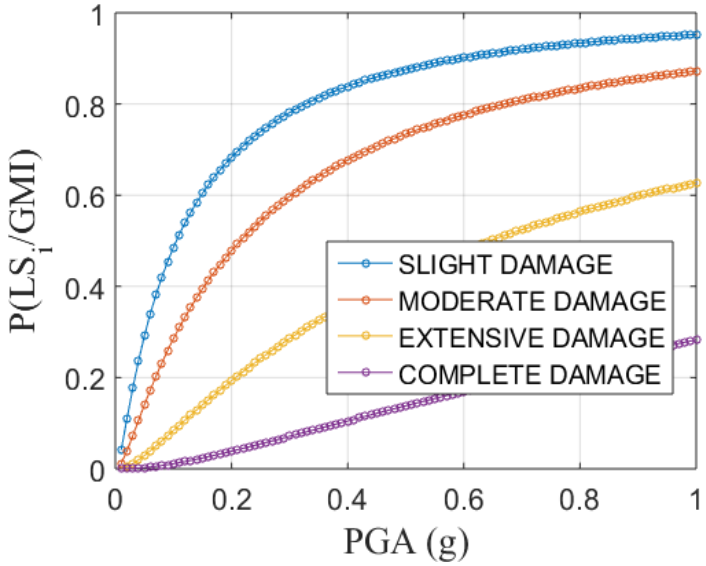

Figure 5-16: Fragility Curve for SSI case

CHAPTER-6 CONCLUSION AND RECOMENDATIONS

6.1 Conclusions

An analytical study to study the seismic response of steel buildings with soil structure interaction (SSI) effect is done. The finite model was validated through the experimentation performed by Xiong et al. (2015). Pushover analysis was done for the generation of capacity curves, which was later utilized to develop fragility function through capacity spectrum method. Based on the work done, the following conclusions were drawn:

i. The time period of the building increases with the consideration of the flexible base footing. For the same height of the building, the base shear for the fixed base footing is more than the flexible base footing. Displacement and drift values for SSI is also comparatively more than that in the fixed base case.
ii. From the push-over analysis, the drift of the building is maximum for the first story of the building with concentration of all plastic hinges at the first story columns.
iii. The SSI case models are found sensitive and more vulnerable at the slight and moderate damage levels limit states over their fixed base counterparts. For extensive and complete damage limit states, both the fixed base and SSI case buildings do not have significant difference in their response.

6.2 Recommendations for Future Work

i. Braced frame system may be used in steel building for comparison purpose in further study.
ii. A detailed time history analysis can be used for further study for fragility function generation.
iii. Frequency dependent spring stiffness and dashpot damping along all six DOF for foundation can be used.

REFERENCES

ATC (1996), "Seismic Evaluation and Retrofit of Concrete Building," *Report* (*ATC-40*), Applied Technology Council, California, Vol. 1, USA.

Awlla, H. A., Taher, N. R., & Mawlood, Y. I. (2020). Effect of Fixed-Base and Soil Structure Interaction on the Dynamic Responses of Steel Structures. *International Journal*, *8*(9).

Chowdhury, P. (2011). Seismic response of low-rise steel moment-resisting frame (SMRF) buildings incorporating nonlinear soil–structure interaction (SSI). *Engineering Structures*, *33*(3), 958-967.

Chhetri, S. K., & Thapa, K. B. (2015). Soil Structure Interaction and Seismic Design Code Provision. *Proceedings of IOE Graduate Conference*, 75-87

FEMA (2000). Prestandard and Commentary for the Seismic Rehabilitation of Buildings, FEMA-356, Washington, D.C

FEMA (2003), HAZUS®MH MR4 Earthquake Model Technical Manual, Department of Homeland Security, FEMA Mitigation Division, Washington, D.C.

Fernandez-Sola, L. R., Davalos-Chavez, D., & Tapia-Hernandez, E. (2014). Influence of the Dynamic Soil Structure Interaction on the Inelastic Response of Steel Frames. In *10th US National Conference on Earthquake Engineering*.

Gazetas, G. (1991). Formulas and charts for impedances of surface and embedded foundations. *Journal of geotechnical engineering*, *117*(9), 1363-1381.

IS 808:1989 Dimensions for Hot Rolled Steel Beam, Column, Channel and Angle Section.

IS 1893:2016 (Part 1) – Criteria for Earthquake Resistant Design of Structures.

Katsimpini, P. S., Papagiannopoulos, G. A., Askouni, P. K., & Karabalis, D. L. (2020). Seismic response of low-rise 3-D steel structures equipped with the seesaw system. *Soil Dynamics and Earthquake Engineering*, *128*, 105877.

NIST (2012). *Soil Structure Interaction for Building Structures.* National Institute of Science and Technology.

NBC:105 (2020) National Building Code. Seismic Design of Building in Nepal

Paul, T. (2014). Resonance effect due to soil structure interaction during earthquakes.

Poudel (2020) Soil Structure Interaction of Soft Story Building in Kathmandu Valley. *Proceedings of IOE Graduate Conference, 8,913-917*

Porter K. (2016) A beginner's guide to fragility, vulnerability, and risk. University of Colorado Boulder, Denver, Colorado, USA.

Pradhan, J.M. (2002) Analytical modelling for soilstructure interaction based on the direct method. *MSC Thesis IOE, Nepal*

Shang, S., Zou, X., & Cao, W. (2012). Experimental investigation on soil-structure interaction of steel frame-raft foundation [J]. *Journal of Building Structures*, *9*.

Shrestha, K. (2011) Development of seismic retrofitting techniques for historical masonry structures with application of high performance materials.

Thapa, S. (2017). Seismic response of RC frame building with soft first storey considering Soil Structure Interaction. *Proceedings of IOE Graduate Conference, 5*, 427-430

Tripathi, A., & Rai, D. C. (2019). Seismic vulnerability assessment and fragility analysis of stone masonry monastic temples in Sikkim Himalayas. *International Journal of Architectural Heritage*, *13*(2), 257-272.

Wen et al.(2004) Vulnerability Function Framework For Consequence based Engineering.

Wolf, J. P. (1985). *Dynamic Soil- Structure Interaction.* New Jersey 07632: Prentice-Hall.

Xiong, W., Jiang, L. Z., & Li, Y. Z. (2016). Influence of soil–structure interaction (structure-to-soil relative stiffness and mass ratio) on the fundamental period of buildings: experimental observation and analytical verification. *Bulletin of Earthquake Engineering*, *14*(1), 139-160.

ANNEX – A

Capacity spectrum method and results for all building cases with fixed base and SSI case

A.1 CSM results for Two and Half story Fixed base case

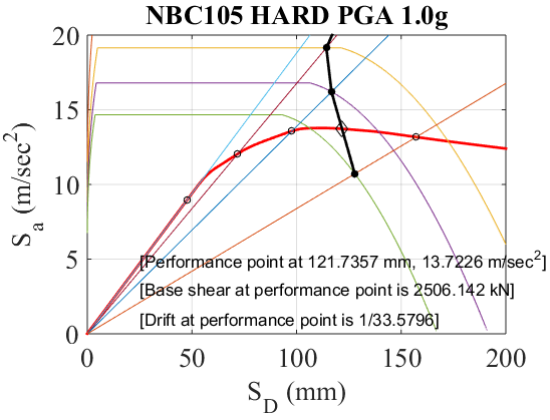

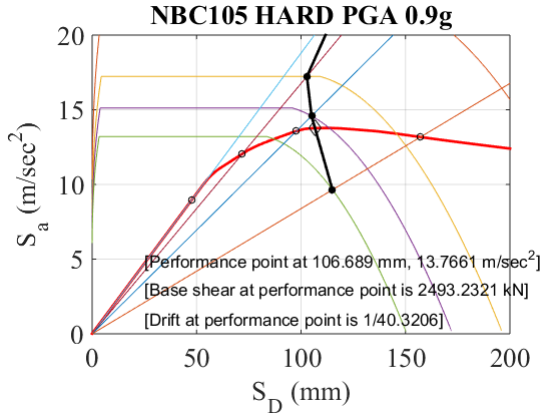

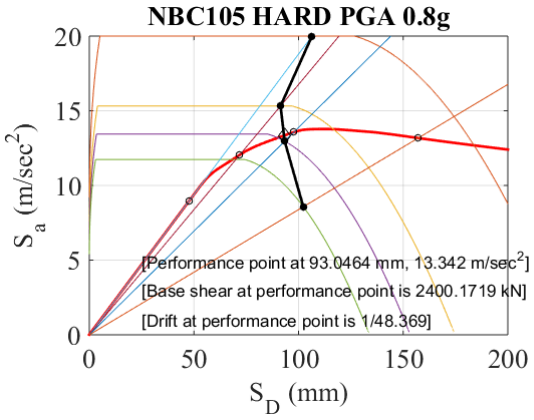

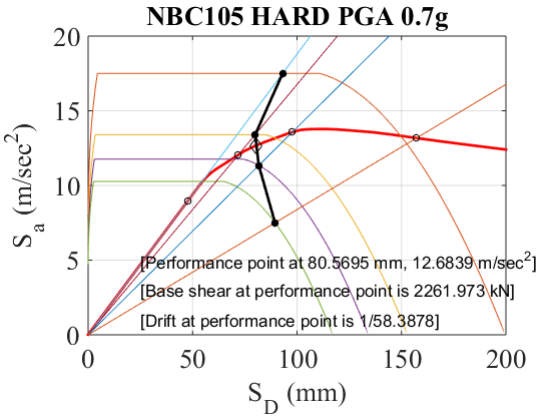

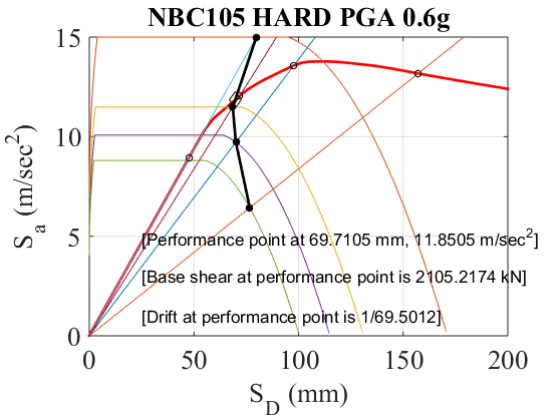

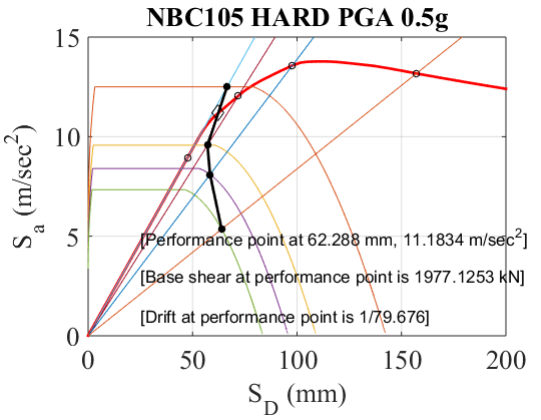

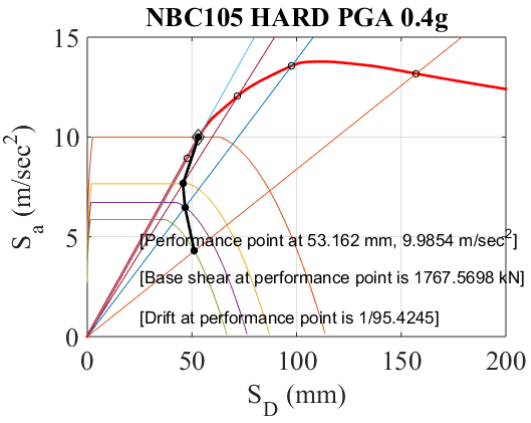
NBC105 HARD PGA 0.4g
[Performance point at 53.162 mm, 9.9854 m/sec^2]
[Base shear at performance point is 1767.5698 kN]
[Drift at performance point is 1/95.4245]
S_a (m/sec^2)
S_D (mm)

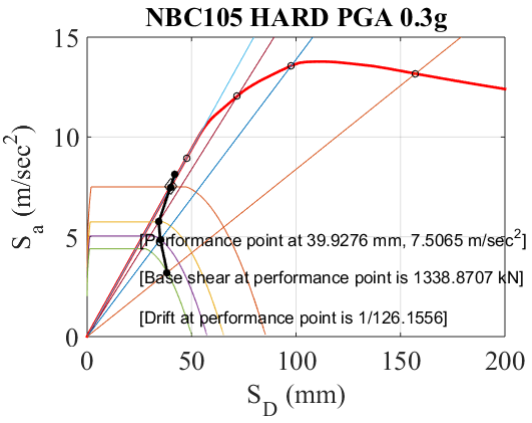
NBC105 HARD PGA 0.3g
[Performance point at 39.9276 mm, 7.5065 m/sec^2]
[Base shear at performance point is 1338.8707 kN]
[Drift at performance point is 1/126.1556]
S_a (m/sec^2)
S_D (mm)

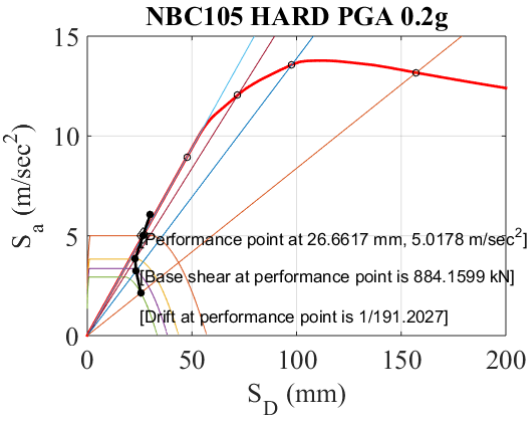
NBC105 HARD PGA 0.2g
[Performance point at 26.6617 mm, 5.0178 m/sec^2]
[Base shear at performance point is 884.1599 kN]
[Drift at performance point is 1/191.2027]
S_a (m/sec^2)
S_D (mm)

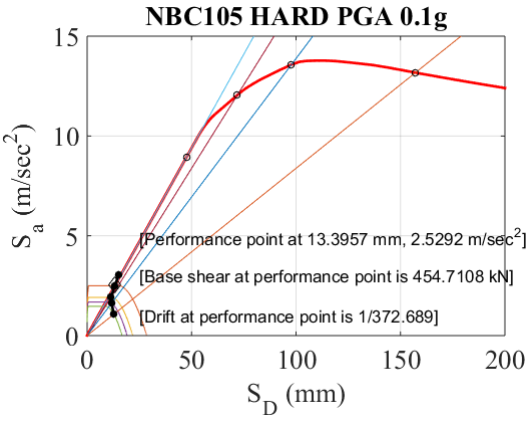
NBC105 HARD PGA 0.1g
[Performance point at 13.3957 mm, 2.5292 m/sec^2]
[Base shear at performance point is 454.7108 kN]
[Drift at performance point is 1/372.689]
S_a (m/sec^2)
S_D (mm)

A.2 CSM results for Two and Half story SSI case

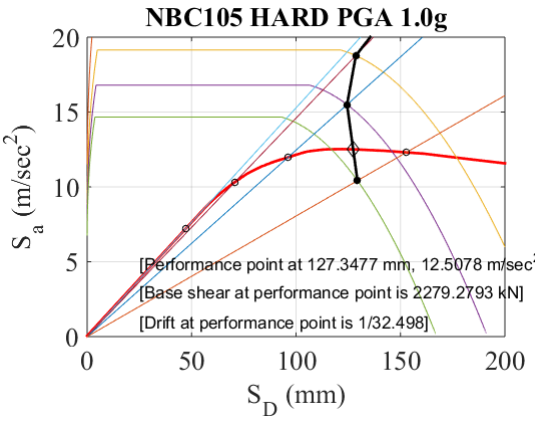

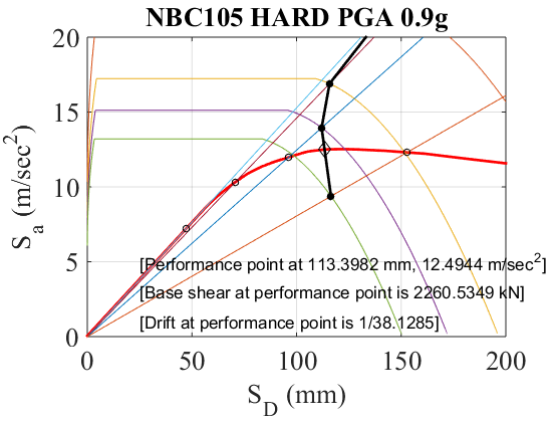

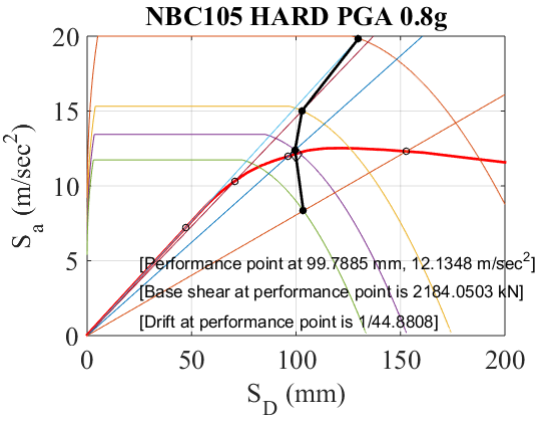

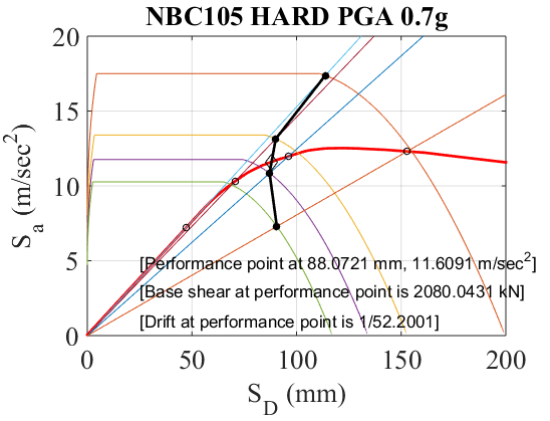

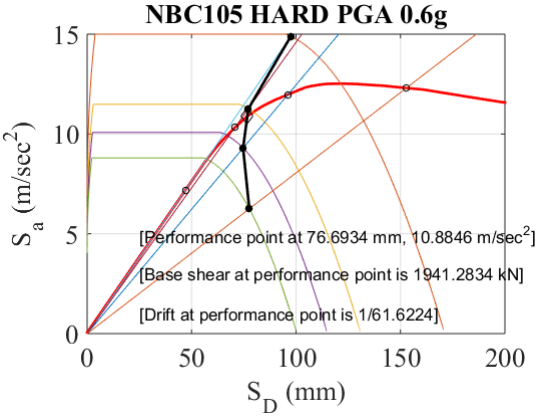

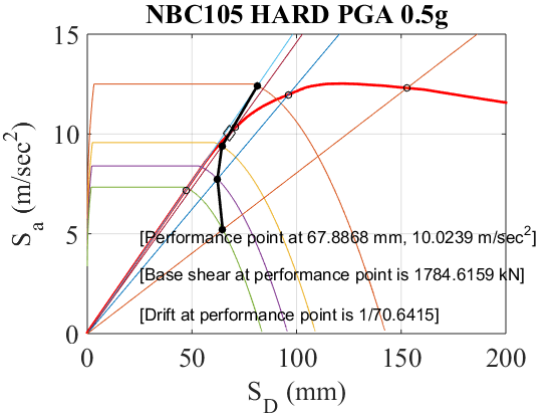

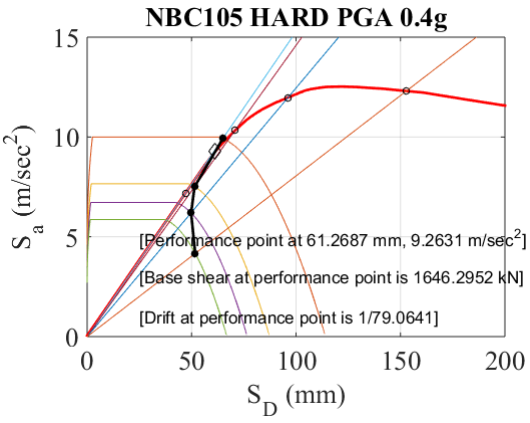
NBC105 HARD PGA 0.4g
[Performance point at 61.2687 mm, 9.2631 m/sec^2]
[Base shear at performance point is 1646.2952 kN]
[Drift at performance point is 1/79.0641]
S_a (m/sec^2)
S_D (mm)

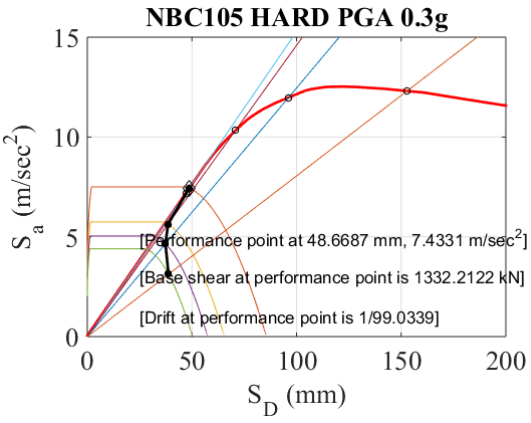
NBC105 HARD PGA 0.3g
[Performance point at 48.6687 mm, 7.4331 m/sec^2]
[Base shear at performance point is 1332.2122 kN]
[Drift at performance point is 1/99.0339]
S_a (m/sec^2)
S_D (mm)

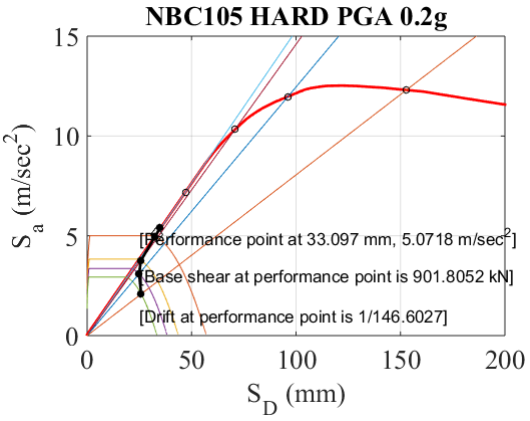
NBC105 HARD PGA 0.2g
[Performance point at 33.097 mm, 5.0718 m/sec^2]
[Base shear at performance point is 901.8052 kN]
[Drift at performance point is 1/146.6027]
S_a (m/sec^2)
S_D (mm)

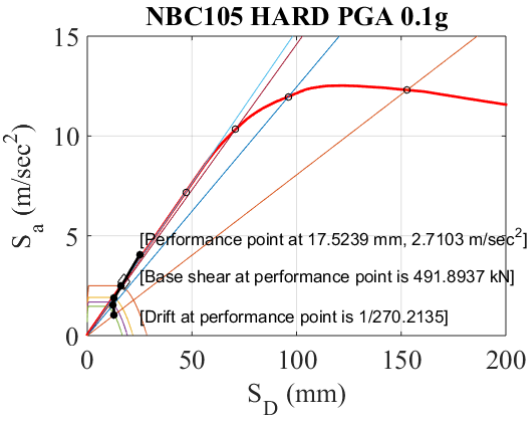
NBC105 HARD PGA 0.1g
[Performance point at 17.5239 mm, 2.7103 m/sec^2]
[Base shear at performance point is 491.8937 kN]
[Drift at performance point is 1/270.2135]
S_a (m/sec^2)
S_D (mm)

A.3 CSM results for Three and Half story Fixed base case

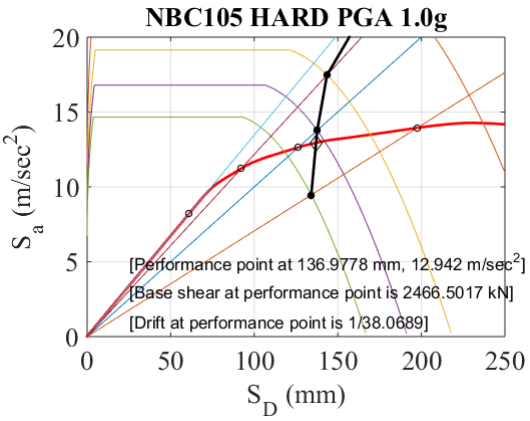

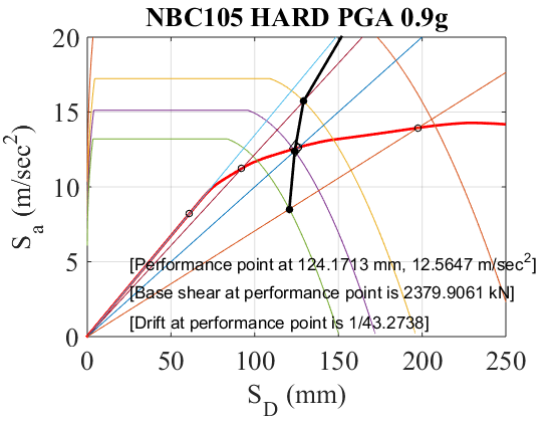

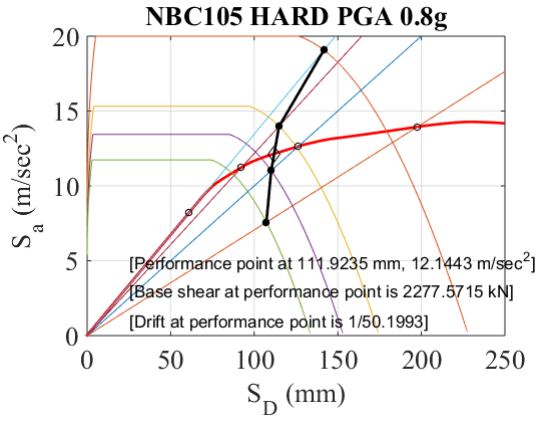

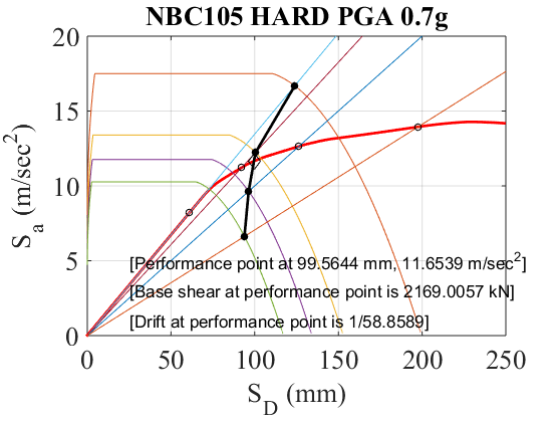

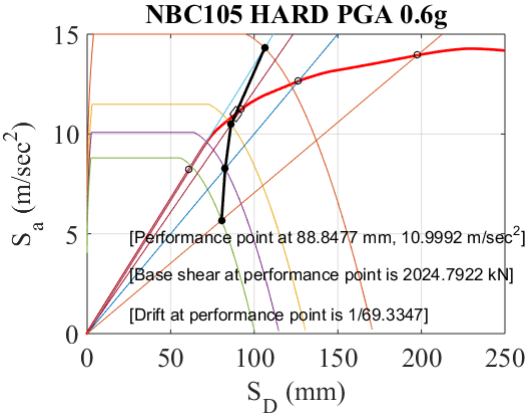

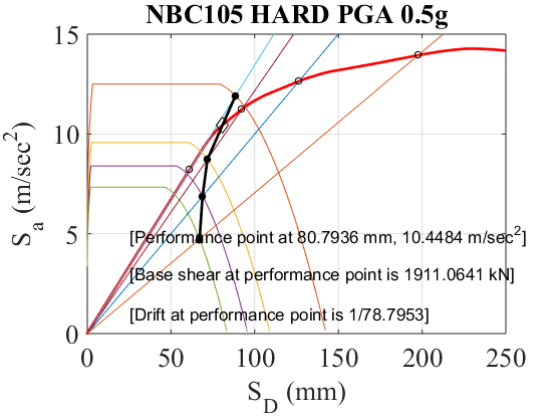

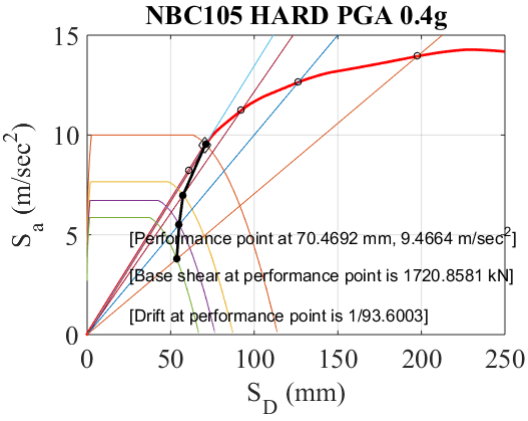
NBC105 HARD PGA 0.4g
S_a (m/sec^2)
S_D (mm)
[Performance point at 70.4692 mm, 9.4664 m/sec^2]
[Base shear at performance point is 1720.8581 kN]
[Drift at performance point is 1/93.6003]

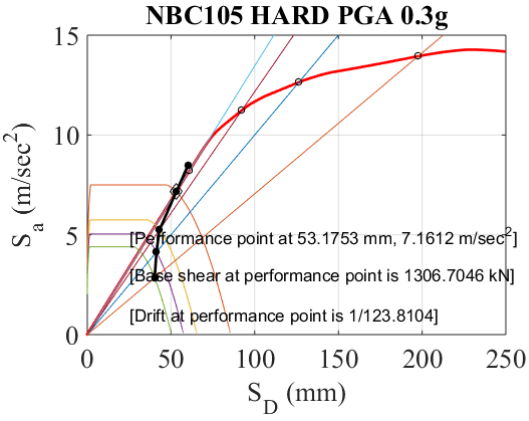
NBC105 HARD PGA 0.3g
S_a (m/sec^2)
S_D (mm)
[Performance point at 53.1753 mm, 7.1612 m/sec^2]
[Base shear at performance point is 1306.7046 kN]
[Drift at performance point is 1/123.8104]

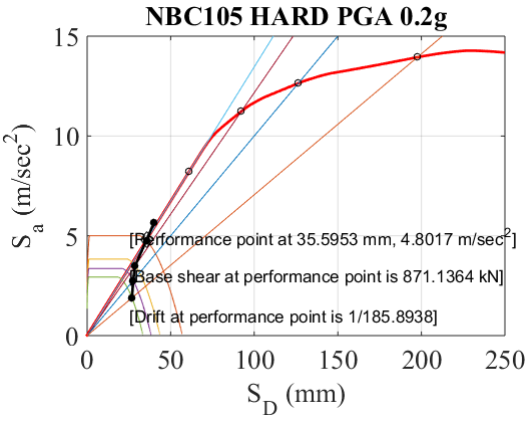
NBC105 HARD PGA 0.2g
S_a (m/sec^2)
S_D (mm)
[Performance point at 35.5953 mm, 4.8017 m/sec^2]
[Base shear at performance point is 871.1364 kN]
[Drift at performance point is 1/185.8938]

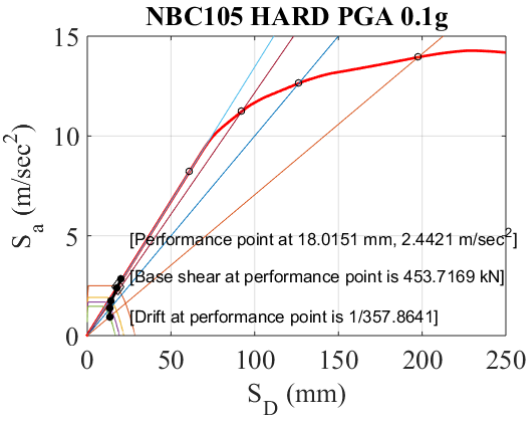
NBC105 HARD PGA 0.1g
S_a (m/sec^2)
S_D (mm)
[Performance point at 18.0151 mm, 2.4421 m/sec^2]
[Base shear at performance point is 453.7169 kN]
[Drift at performance point is 1/357.8641]

A.4 CSM results for Three and Half story SSI case

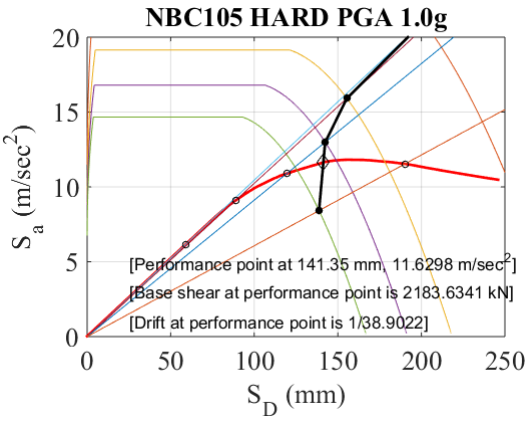

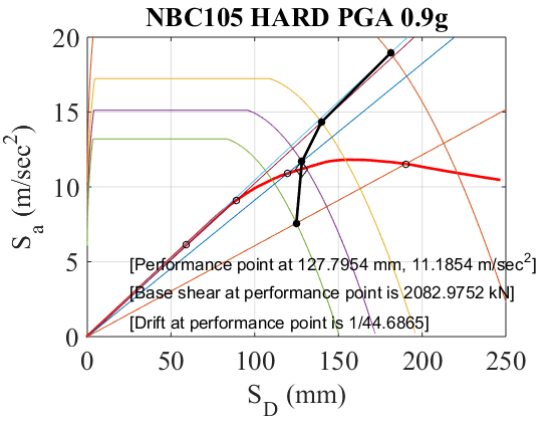

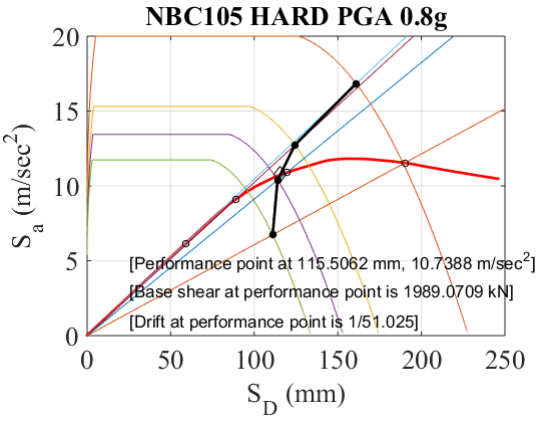

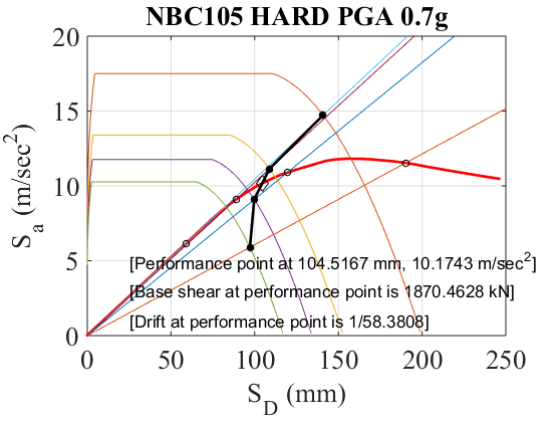

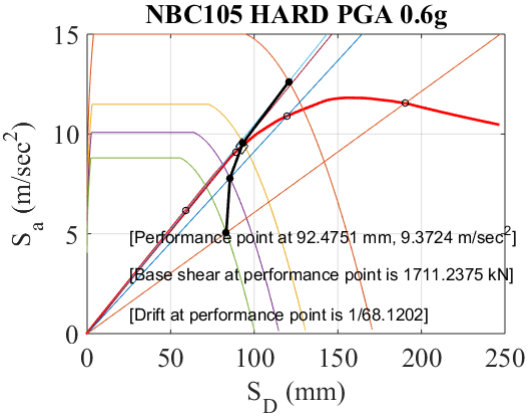

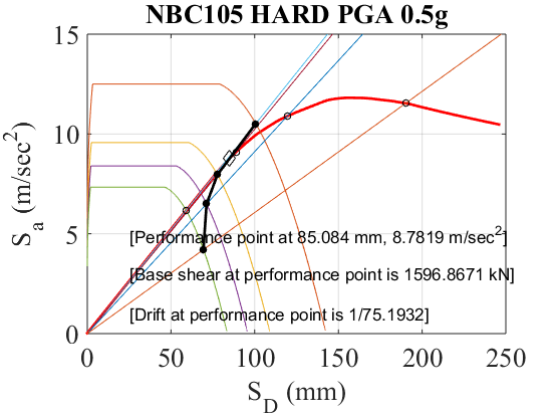

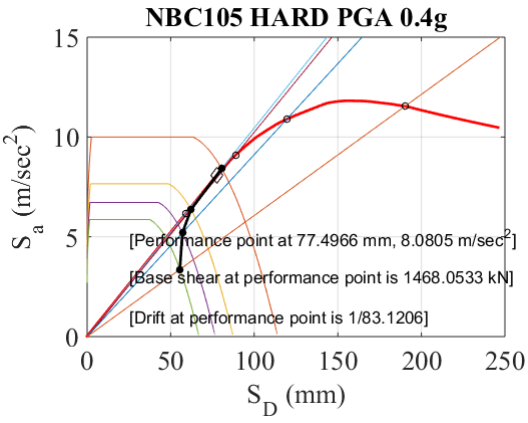
NBC105 HARD PGA 0.4g
[Performance point at 77.4966 mm, 8.0805 m/sec^2]
[Base shear at performance point is 1468.0533 kN]
[Drift at performance point is 1/83.1206]
S_a (m/sec^2)
S_D (mm)

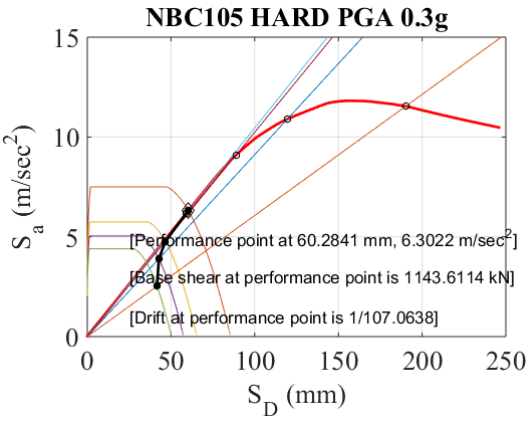
NBC105 HARD PGA 0.3g
[Performance point at 60.2841 mm, 6.3022 m/sec^2]
[Base shear at performance point is 1143.6114 kN]
[Drift at performance point is 1/107.0638]
S_a (m/sec^2)
S_D (mm)

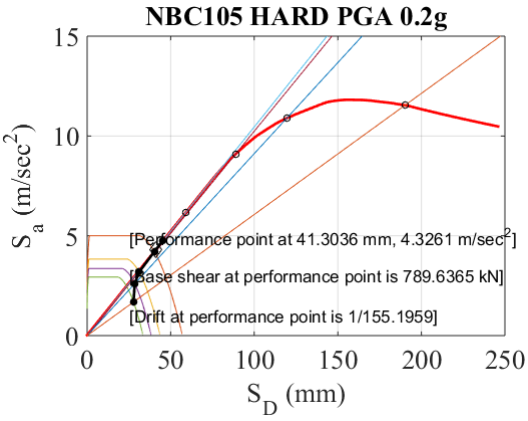
NBC105 HARD PGA 0.2g
[Performance point at 41.3036 mm, 4.3261 m/sec^2]
[Base shear at performance point is 789.6365 kN]
[Drift at performance point is 1/155.1959]
S_a (m/sec^2)
S_D (mm)

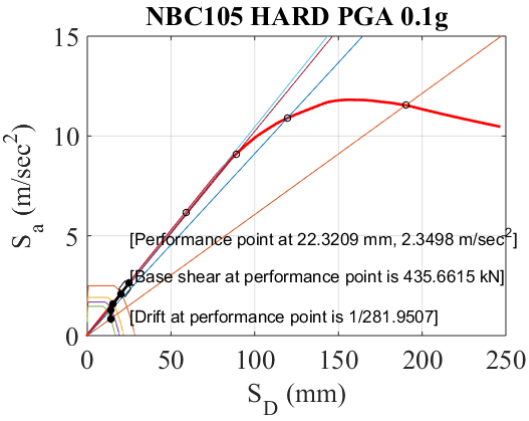
NBC105 HARD PGA 0.1g
[Performance point at 22.3209 mm, 2.3498 m/sec^2]
[Base shear at performance point is 435.6615 kN]
[Drift at performance point is 1/281.9507]
S_a (m/sec^2)
S_D (mm)

A.5 CSM results for Four and Half story Fixed base case

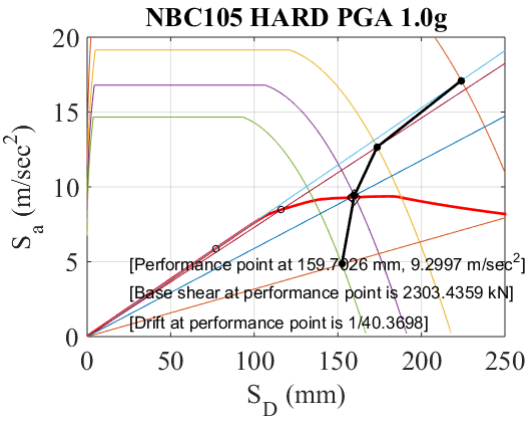

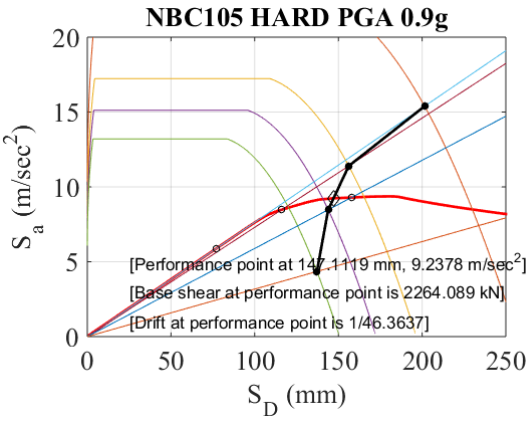

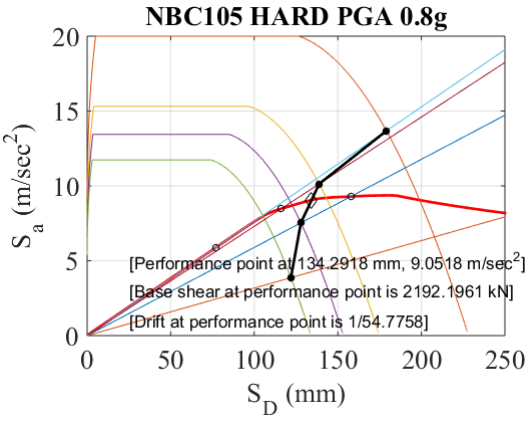

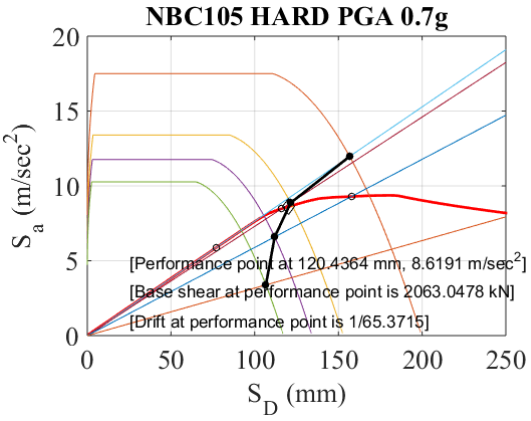

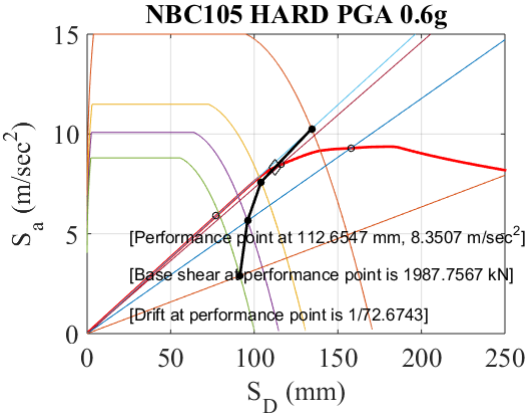

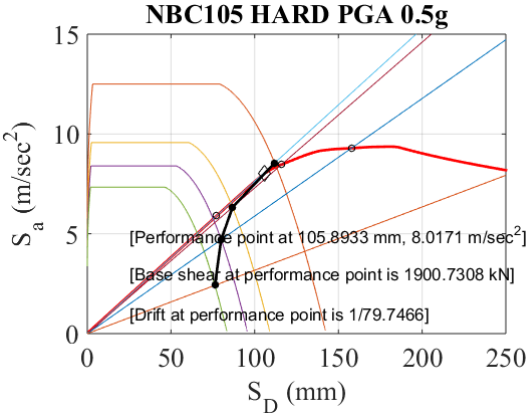

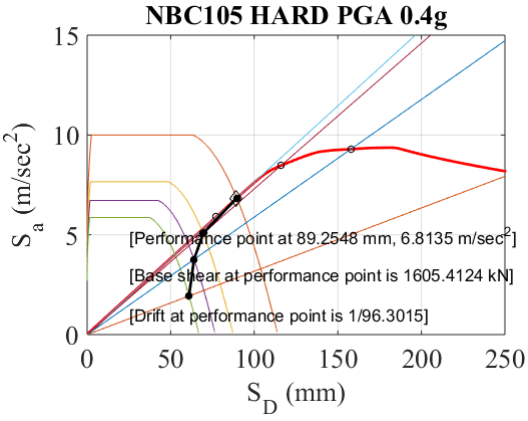
NBC105 HARD PGA 0.4g
[Performance point at 89.2548 mm, 6.8135 m/sec^2]
[Base shear at performance point is 1605.4124 kN]
[Drift at performance point is 1/96.3015]
S_a (m/sec^2)
S_D (mm)

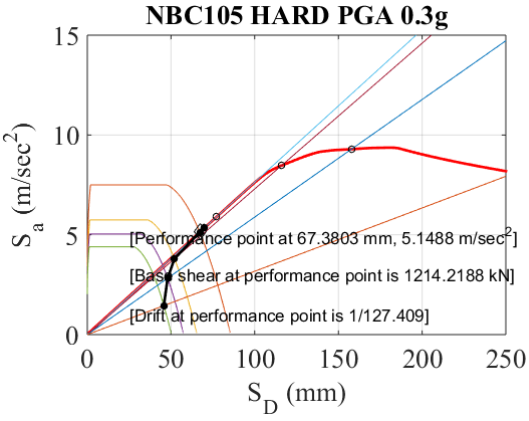
NBC105 HARD PGA 0.3g
[Performance point at 67.3803 mm, 5.1488 m/sec^2]
[Base shear at performance point is 1214.2188 kN]
[Drift at performance point is 1/127.409]
S_a (m/sec^2)
S_D (mm)

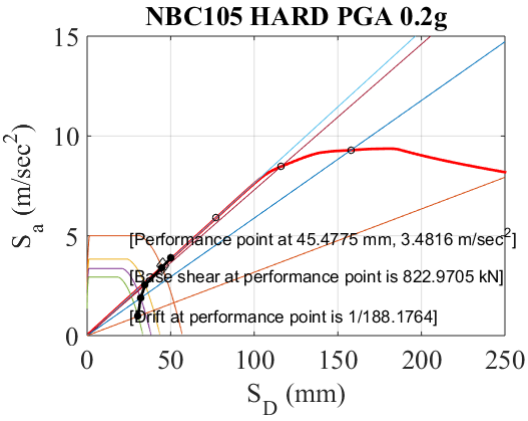
NBC105 HARD PGA 0.2g
[Performance point at 45.4775 mm, 3.4816 m/sec^2]
[Base shear at performance point is 822.9705 kN]
[Drift at performance point is 1/188.1764]
S_a (m/sec^2)
S_D (mm)

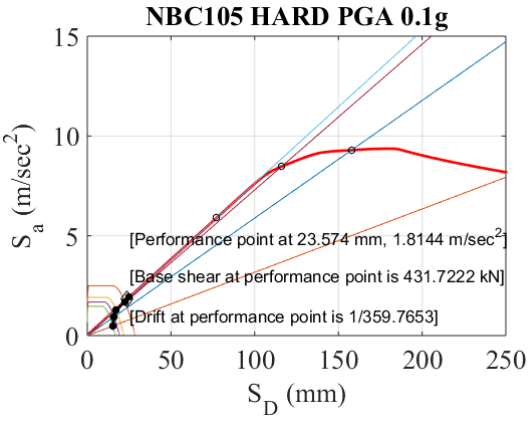
NBC105 HARD PGA 0.1g
[Performance point at 23.574 mm, 1.8144 m/sec^2]
[Base shear at performance point is 431.7222 kN]
[Drift at performance point is 1/359.7653]
S_a (m/sec^2)
S_D (mm)

A.6 CSM results for Four and Half story SSI case

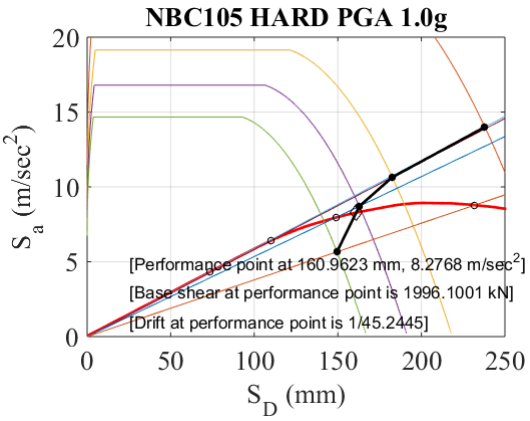

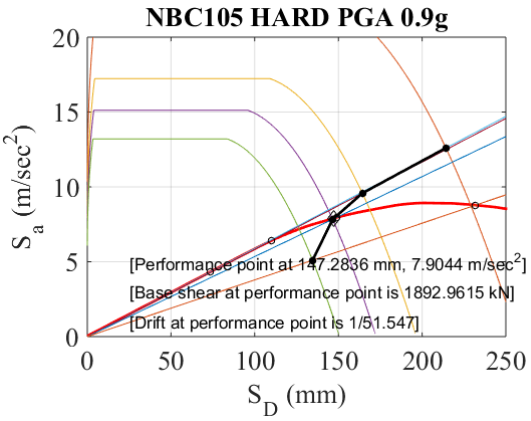

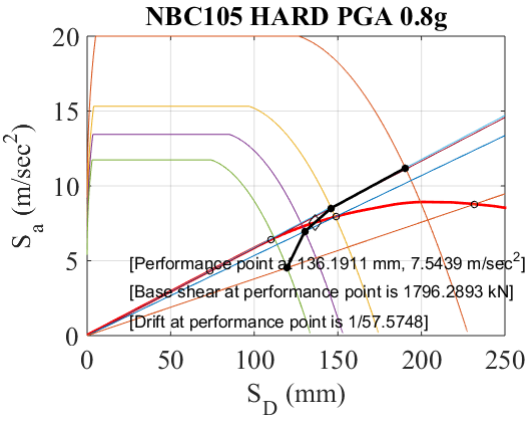

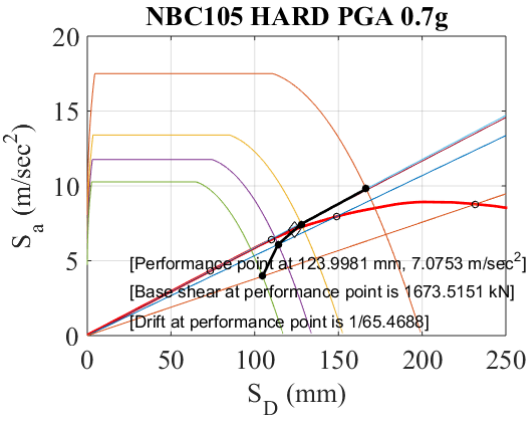

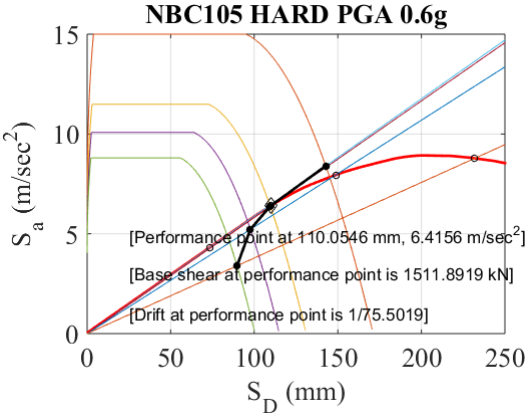

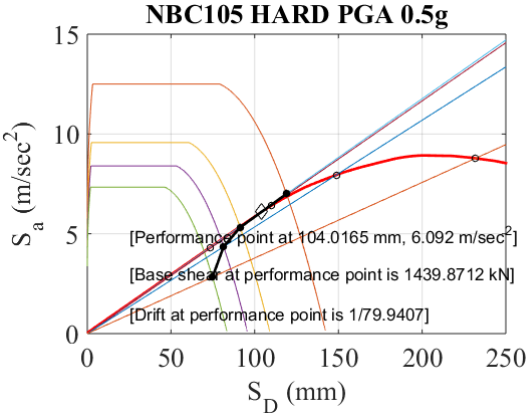

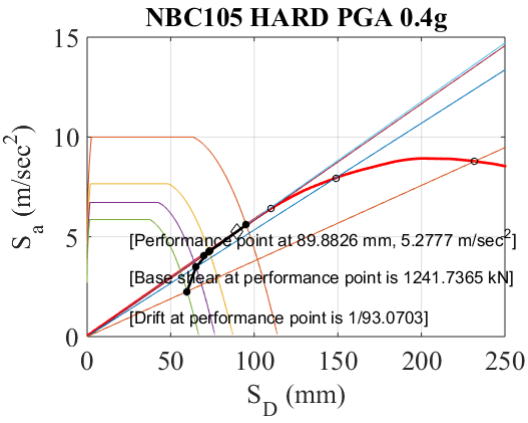
NBC105 HARD PGA 0.4g
[Performance point at 89.8826 mm, 5.2777 m/sec^2]
[Base shear at performance point is 1241.7365 kN]
[Drift at performance point is 1/93.0703]
S_a (m/sec^2)
S_D (mm)

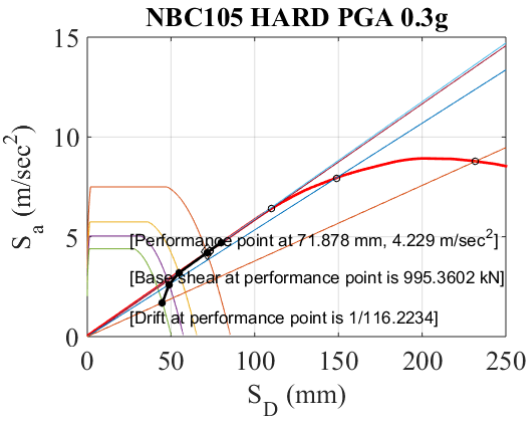
NBC105 HARD PGA 0.3g
[Performance point at 71.878 mm, 4.229 m/sec^2]
[Base shear at performance point is 995.3602 kN]
[Drift at performance point is 1/116.2234]
S_a (m/sec^2)
S_D (mm)

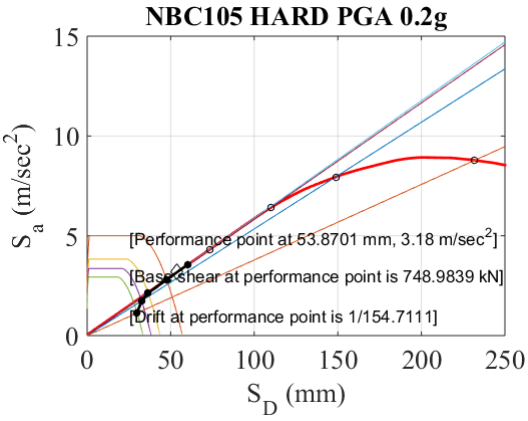
NBC105 HARD PGA 0.2g
[Performance point at 53.8701 mm, 3.18 m/sec^2]
[Base shear at performance point is 748.9839 kN]
[Drift at performance point is 1/154.7111]
S_a (m/sec^2)
S_D (mm)

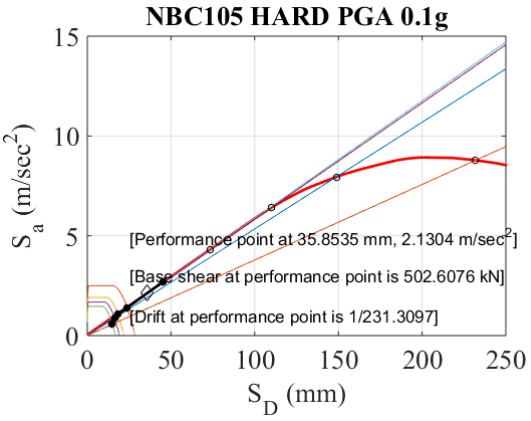
NBC105 HARD PGA 0.1g
[Performance point at 35.8535 mm, 2.1304 m/sec^2]
[Base shear at performance point is 502.6076 kN]
[Drift at performance point is 1/231.3097]
S_a (m/sec^2)
S_D (mm)

A.7 CSM results for Five and Half story Fixed base case

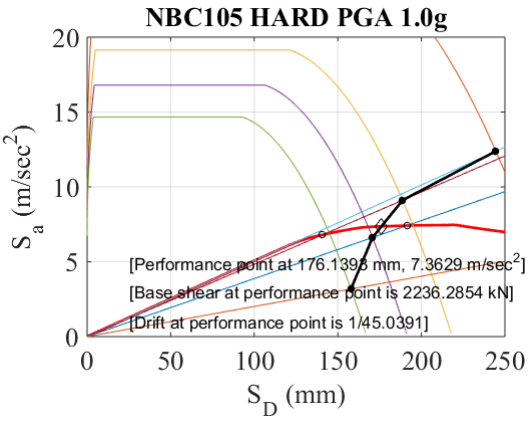

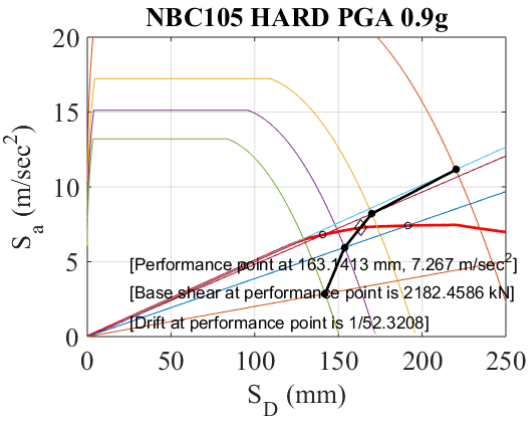

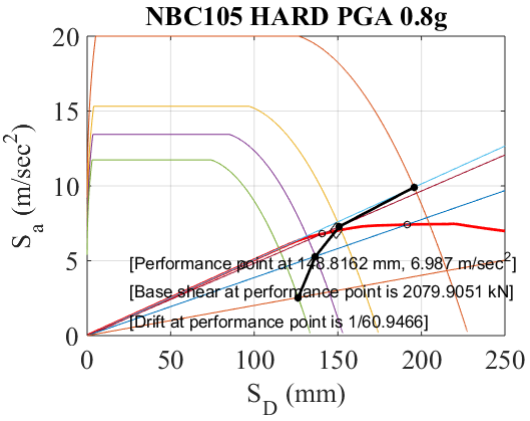

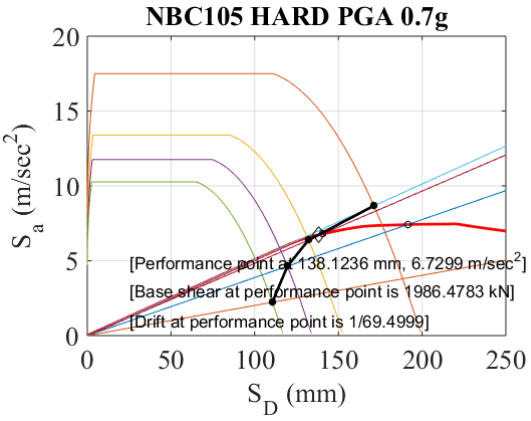

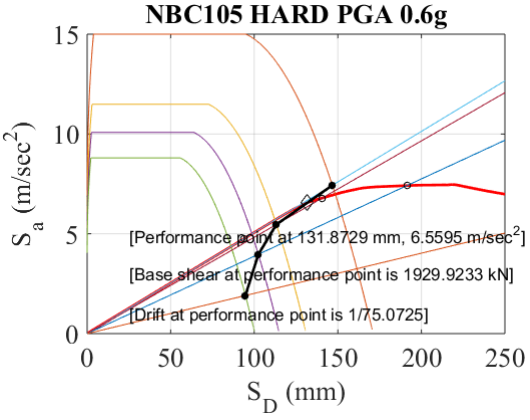

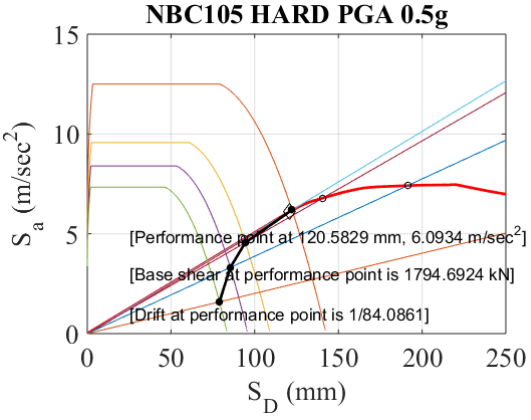

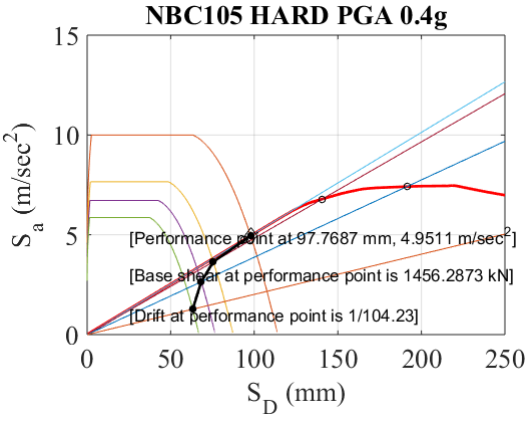
NBC105 HARD PGA 0.4g
[Performance point at 97.7687 mm, 4.9511 m/sec^2]
[Base shear at performance point is 1456.2873 kN]
[Drift at performance point is 1/104.23]
S_a (m/sec^2)
S_D (mm)

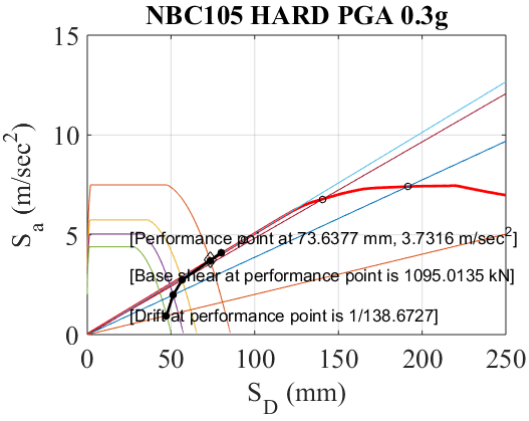
NBC105 HARD PGA 0.3g
[Performance point at 73.6377 mm, 3.7316 m/sec^2]
[Base shear at performance point is 1095.0135 kN]
[Drift at performance point is 1/138.6727]
S_a (m/sec^2)
S_D (mm)

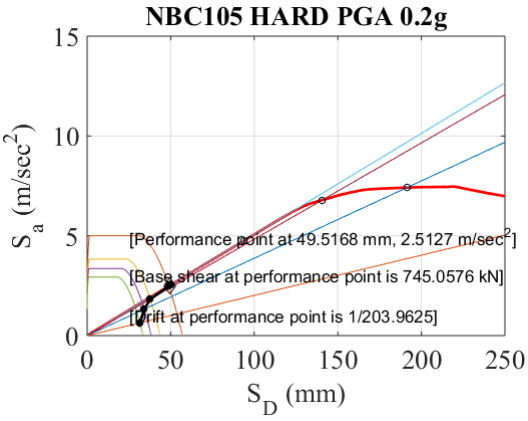
NBC105 HARD PGA 0.2g
[Performance point at 49.5168 mm, 2.5127 m/sec^2]
[Base shear at performance point is 745.0576 kN]
[Drift at performance point is 1/203.9625]
S_a (m/sec^2)
S_D (mm)

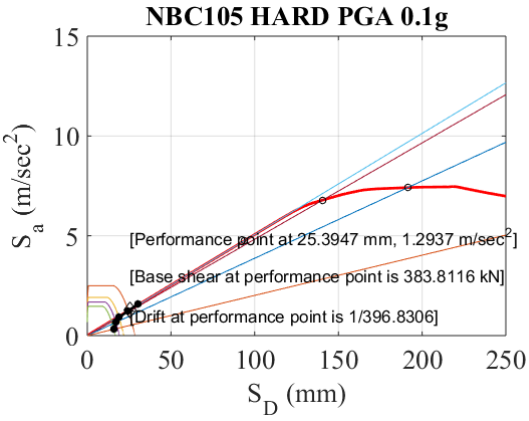
NBC105 HARD PGA 0.1g
[Performance point at 25.3947 mm, 1.2937 m/sec^2]
[Base shear at performance point is 383.8116 kN]
[Drift at performance point is 1/396.8306]
S_a (m/sec^2)
S_D (mm)

A.8 CSM results for Five and Half story SSI case

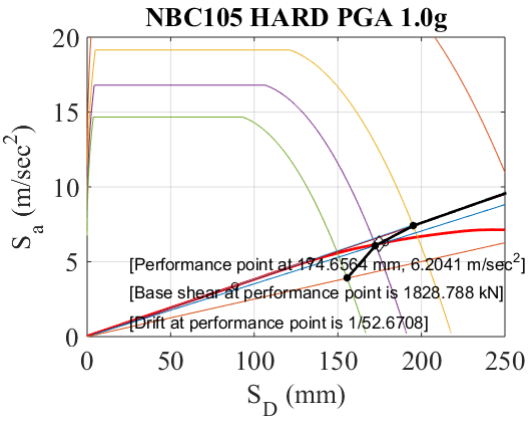

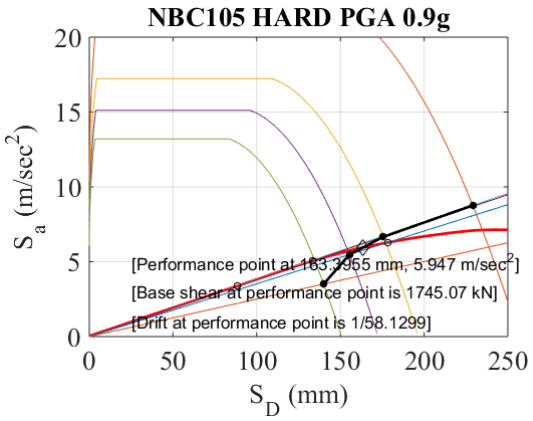

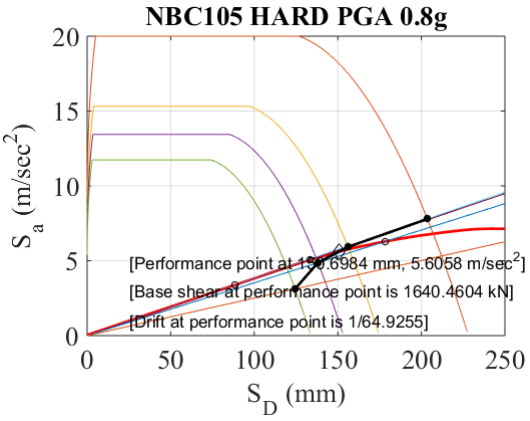

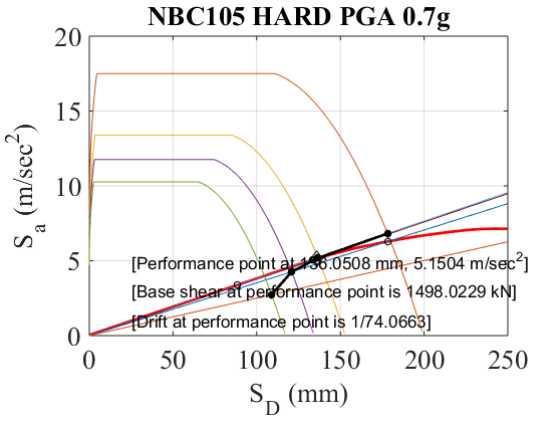

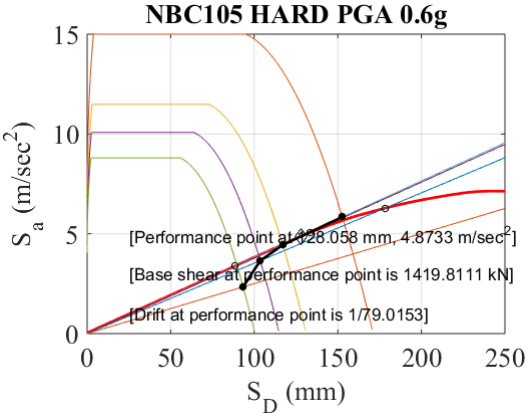

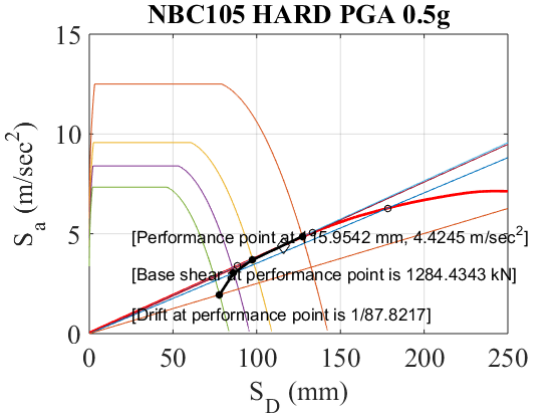

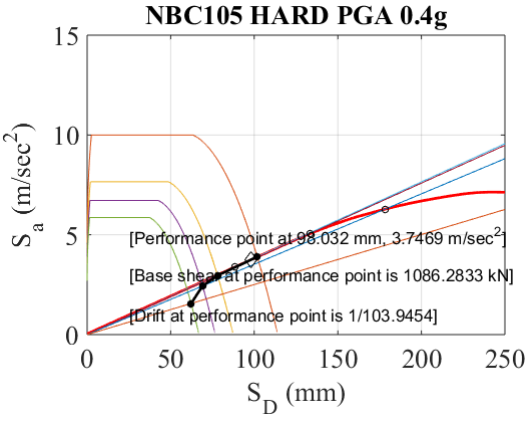
NBC105 HARD PGA 0.4g
[Performance point at 98.032 mm, 3.7469 m/sec^2]
[Base shear at performance point is 1086.2833 kN]
[Drift at performance point is 1/103.9454]
S_a (m/sec^2)
S_D (mm)

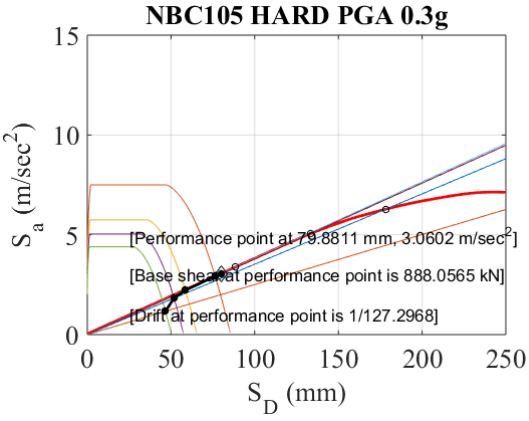
NBC105 HARD PGA 0.3g
[Performance point at 79.8811 mm, 3.0602 m/sec^2]
[Base shear at performance point is 888.0565 kN]
[Drift at performance point is 1/127.2968]
S_a (m/sec^2)
S_D (mm)

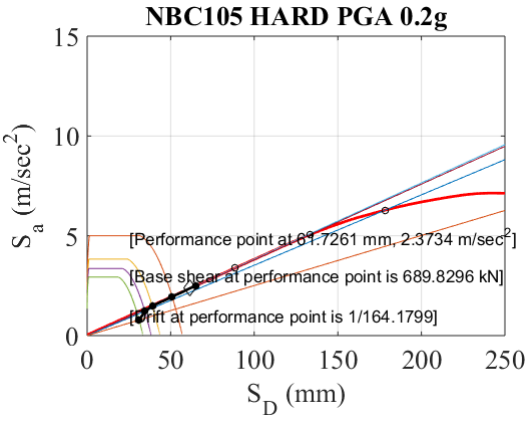
NBC105 HARD PGA 0.2g
[Performance point at 61.7261 mm, 2.3734 m/sec^2]
[Base shear at performance point is 689.8296 kN]
[Drift at performance point is 1/164.1799]
S_a (m/sec^2)
S_D (mm)

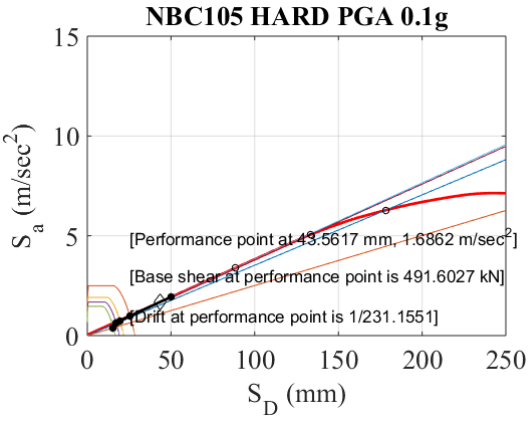
NBC105 HARD PGA 0.1g
[Performance point at 43.5617 mm, 1.6862 m/sec^2]
[Base shear at performance point is 491.6027 kN]
[Drift at performance point is 1/231.1551]
S_a (m/sec^2)
S_D (mm)

ANNEX – B

Spring constants for SSI based models:

B.1 Three and half story building

Table B.1.1 Total dynamic stiffness values for three and half story building

TOTAL STIFFNESS OF THREE AND HALF STORY (kN/m)					
KZ	KY	KX	KXX	KYY	KZZ
714196.7	579489.7	574157.7	23231380	27072334	45015081

Table B.1.2 Dynamic stiffness values for individual columns of three and half story building

Three and Half Story Building Stiffness (kN/m)						
column	kz	ky	kx	kxx	kyy	kzz
1	20621.47	20621.47	16578.03	670774.7	781677.1	1299750
2	43305.08	43305.08	34813.86	1408627	1641522	2729474
3	49492.19	49492.19	39787.81	1609881	1876051	3119442
4	26808.58	26808.58	21551.98	872029.1	1016206	1689717
5	30932.2	30932.2	24867.04	1006162	1172516	1949624
6	64957.62	64957.62	52220.79	2112940	2462283	4094211
7	74238.29	74238.29	59681.72	2414822	2814076	4679163
8	46399.31	46399.31	37301.38	1509276	1758812	2924501
9	6186.44	6186.44	4973.408	201232.4	234503.1	389924.9
10	19332.62	19332.62	15541.9	628851.3	732822.2	1218515
11	59544.48	59544.48	47869.05	1936862	2257092	3753027
12	68051.77	68051.77	54708.24	2213587	2579570	4289232
13	43048.24	43048.24	34607.38	1400272	1631786	2713286
14	6186.44	6186.44	4973.408	201232.4	234503.1	389924.9
15	19762.24	19762.24	15887.28	642825.7	749107.2	1245593
16	10740.35	10740.35	8634.389	349361.8	407123.5	676952.9
17	45109.46	45109.46	36264.44	1467320	1709919	2843202
18	51554.37	51554.37	41445.64	1676960	1954219	3249418
19	27925.61	27925.61	22449.98	908363.6	1058548	1760122

Table B.1.3. Total damping constant values for three and half story building

TOTAL DAMPING OF THREE AND HALF STORY (kN S/m)					
CZ	CY	CX	CXX	CYY	CZZ
48644.61	28302.58	31447.31	69633.83	104123.1	101110

Table B.1.4. Damping constants for individual columns of three and half story building

Three and Half Story Building Damping Constant(kN s/m)						
column	cz	cy	cx	cxx	cyy	czz
1	1404.547	817.1986	907.9985	2010.583	3006.414	2919.414
2	2949.549	1716.117	1906.797	4222.224	6313.469	6130.77
3	3370.96	1961.304	2179.226	4825.465	7215.492	7006.69
4	1825.958	1062.385	1180.428	2613.824	3908.437	3795.334
5	2106.821	1225.798	1361.998	3015.874	4509.621	4379.122
6	4424.324	2574.176	2860.195	6333.336	9470.203	9196.155
7	5056.439	2941.955	3268.839	7238.197	10823.24	10510.04
8	3160.3	1838.737	2043.041	4523.91	6764.579	6568.826
9	421.3642	245.1596	272.3995	603.1748	901.9241	875.8243
10	1316.763	766.1237	851.2486	1884.921	2818.513	2736.951
11	4055.63	2359.661	2621.846	5805.558	8681.02	8429.809
12	4635.069	2696.792	2996.436	6635.014	9921.301	9634.199
13	2932.056	1705.939	1895.488	4197.182	6276.024	6094.409
14	421.3642	245.1596	272.3995	603.1748	901.9241	875.8243
15	1346.024	783.1487	870.1652	1926.808	2881.147	2797.772
16	731.535	425.6243	472.9159	1047.179	1565.841	1520.528
17	3072.447	1787.622	1986.247	4398.15	6576.53	6386.219
18	3511.416	2043.025	2270.027	5026.526	7516.137	7298.636
19	1902.039	1106.651	1229.612	2722.733	4071.288	3953.473

B.2 Four and half story building

Table B.2.1 Total dynamic stiffness values for three and half story building

TOTAL STIFFNESS OF THREE AND HALF STORY (kN/m)					
KZ	KY	KX	KXX	KYY	KZZ
714196.7	579489.7	574157.7	24140956	28501532	46206103

Table B.2.2 Dynamic stiffness values for individual columns of three and half story building

Four and Half Story Building Stiffness Constant(kN/m)						
column	kz	ky	kx	kxx	kyy	kzz
1	20621.47	20621.47	16578.03	697037.5	822943.2	1334139
2	43305.08	43305.08	34813.86	1463779	1728181	2801691
3	49492.19	49492.19	39787.81	1672913	1975091	3201977
4	26808.58	26808.58	21551.98	906171.6	1069853	1734424
5	30932.2	30932.2	24867.04	1045556	1234415	2001208
6	64957.62	64957.62	52220.79	2195668	2592271	4202537
7	74238.29	74238.29	59681.72	2509369	2962636	4802965
8	46399.31	46399.31	37301.38	1568369	1851663	3001878
9	6186.44	6186.44	4973.408	209111.2	246883	400241.6
10	19332.62	19332.62	15541.9	653472.6	771509.3	1250755
11	59544.48	59544.48	47869.05	2012696	2376248	3852326
12	68051.77	68051.77	54708.24	2300255	2715750	4402718
13	43048.24	43048.24	34607.38	1455097	1717931	2785075
14	6186.44	6186.44	4973.408	209111.2	246883	400241.6
15	19762.24	19762.24	15887.28	667994.2	788653.9	1278550
16	10740.35	10740.35	8634.389	363040.3	428616.3	694863.9
17	45109.46	45109.46	36264.44	1524769	1800188	2918429
18	51554.37	51554.37	41445.64	1742617	2057386	3335392
19	27925.61	27925.61	22449.98	943928.7	1114430	1806692

Table B.2.3. Total damping constant values for four and half story building

TOTAL DAMPING OF FOUR AND HALF STORY (kN S/m)					
CZ	CY	CX	CXX	CYY	CZZ
48644.61	28302.58	31447.31	69633.83	104123.1	101110

Table B.2.4. Damping constants for individual columns of four and half story building

Four and Half Story Building Damping Constant						
column	cz	cy	cx	cxx	cyy	czz
1	1404.547	817.1986	907.9985	2010.583	3006.414	2919.414
2	2949.549	1716.117	1906.797	4222.224	6313.469	6130.77
3	3370.96	1961.304	2179.226	4825.465	7215.492	7006.69
4	1825.958	1062.385	1180.428	2613.824	3908.437	3795.334
5	2106.821	1225.798	1361.998	3015.874	4509.621	4379.122
6	4424.324	2574.176	2860.195	6333.336	9470.203	9196.155
7	5056.439	2941.955	3268.839	7238.197	10823.24	10510.04
8	3160.3	1838.737	2043.041	4523.91	6764.579	6568.826
9	421.3642	245.1596	272.3995	603.1748	901.9241	875.8243
10	1316.763	766.1237	851.2486	1884.921	2818.513	2736.951
11	4055.63	2359.661	2621.846	5805.558	8681.02	8429.809
12	4635.069	2696.792	2996.436	6635.014	9921.301	9634.199
13	2932.056	1705.939	1895.488	4197.182	6276.024	6094.409
14	421.3642	245.1596	272.3995	603.1748	901.9241	875.8243
15	1346.024	783.1487	870.1652	1926.808	2881.147	2797.772
16	731.535	425.6243	472.9159	1047.179	1565.841	1520.528
17	3072.447	1787.622	1986.247	4398.15	6576.53	6386.219
18	3511.416	2043.025	2270.027	5026.526	7516.137	7298.636
19	1902.039	1106.651	1229.612	2722.733	4071.288	3953.473

B.3 Five and half story building

Table B.3.1 Total dynamic stiffness values for five and half story building

TOTAL STIFFNESS OF THREE AND HALF STORY (kN/m)					
KZ	KY	KX	KXX	KYY	KZZ
714196.7	579489.7	574157.7	24415537	28932976	46565647

Table B.3.2 Dynamic stiffness values for individual columns of five and half story building

Five and Half Story Stiffness Constant (kN/m)						
column	kz	ky	kx	kxx	kyy	kzz
1	20621.47	20621.47	16578.03	704965.6	835400.6	1344520
2	43305.08	43305.08	34813.86	1480428	1754341	2823492
3	49492.19	49492.19	39787.81	1691941	2004989	3226892
4	26808.58	26808.58	21551.98	916478.5	1086048	1747920
5	30932.2	30932.2	24867.04	1057448	1253101	2016780
6	64957.62	64957.62	52220.79	2220642	2631512	4235238
7	74238.29	74238.29	59681.72	2537911	3007483	4840339
8	46399.31	46399.31	37301.38	1586207	1879692	3025236
9	6186.44	6186.44	4973.408	211489.7	250620.2	403356
10	19332.62	19332.62	15541.9	660905.3	783188	1260488
11	59544.48	59544.48	47869.05	2035588	2412219	3882302
12	68051.77	68051.77	54708.24	2326418	2756860	4436977
13	43048.24	43048.24	34607.38	1471648	1743936	2806746
14	6186.44	6186.44	4973.408	211489.7	250620.2	403356
15	19762.24	19762.24	15887.28	675592.1	800592.2	1288498
16	10740.35	10740.35	8634.389	367169.6	435104.5	700270.9
17	45109.46	45109.46	36264.44	1542112	1827439	2941138
18	51554.37	51554.37	41445.64	1762438	2088530	3361346
19	27925.61	27925.61	22449.98	954665.1	1131300	1820750

Table B.3.3. Total damping constant values for five and half story building

TOTAL DAMPING OF FIVE AND HALF STORY (kN s/m)					
CZ	CY	CX	CXX	CYY	CZZ
48644.61	28302.58	31447.31	69633.83	104123.1	101110

Table B.3.4. Damping constants for individual columns of five and half story building

Five and Half Story Damping Constant (kN s/m)						
column	cz	cy	cx	cxx	cyy	czz
1	1404.547	817.1986	907.9985	2010.583	3006.414	2919.414
2	2949.549	1716.117	1906.797	4222.224	6313.469	6130.77
3	3370.96	1961.304	2179.226	4825.465	7215.492	7006.69
4	1825.958	1062.385	1180.428	2613.824	3908.437	3795.334
5	2106.821	1225.798	1361.998	3015.874	4509.621	4379.122
6	4424.324	2574.176	2860.195	6333.336	9470.203	9196.155
7	5056.439	2941.955	3268.839	7238.197	10823.24	10510.04
8	3160.3	1838.737	2043.041	4523.91	6764.579	6568.826
9	421.3642	245.1596	272.3995	603.1748	901.9241	875.8243
10	1316.763	766.1237	851.2486	1884.921	2818.513	2736.951
11	4055.63	2359.661	2621.846	5805.558	8681.02	8429.809
12	4635.069	2696.792	2996.436	6635.014	9921.301	9634.199
13	2932.056	1705.939	1895.488	4197.182	6276.024	6094.409
14	421.3642	245.1596	272.3995	603.1748	901.9241	875.8243
15	1346.024	783.1487	870.1652	1926.808	2881.147	2797.772
16	731.535	425.6243	472.9159	1047.179	1565.841	1520.528
17	3072.447	1787.622	1986.247	4398.15	6576.53	6386.219
18	3511.416	2043.025	2270.027	5026.526	7516.137	7298.636
19	1902.039	1106.651	1229.612	2722.733	4071.288	3953.473

ANNEX –C

Calculation of the Stiffness and the Damping of the Foundation

Given parameters

2L=12.1921m, B=13.106m, $A_{b=}$ 111.48m^2, ϑ=0.3, V_s=100m/s

T=0.375 sec

Calculation

$\omega = \frac{2*\pi}{T}$ ==16.74 rad/sec

V_s=100 m/s

$a_0 = \frac{\omega x B}{V_s} = \frac{16.74x4.572}{100}$ =0.765

ρ =1.64g/cm^3 =1640kg/m^3

G=ρ x V_s x V_s =16400000N/m^2

$\chi = {}^{A_b}/_{4L^2} = {}^{111.48}/_{4x6.096^2}$

Total Static Stiffness

$$K_z = \left[\frac{2GL}{(1-\vartheta)}\right](0.73+1.54\chi^{0.75})$$

=556,991.030 kN/m

Dynamic Stiffness Coefficient

From the graph we get,

Dynamic stiffness coefficient=0.97

Total Dynamic Stiffness

= Dynamic stiffness coefficient x Total Static Stiffness

=0.97 x 556,991.030

=540281.3 kN/m